https://ntrs.nasa.gov/search.jsp?R=19650023769 2019-01-07T23:37:18+00:00Z

NASA-CR-65142

COMBINED SPACE ENVIRONMENT EFFECTS ON TYPICAL SPACECRAFT WINDOW MATERIALS

July, 1965

FINAL REPORT

Contract NAS9-2939

TR 65-351-F

FACILITY FORM 602

N65-33370 (ACCESSION NUMBER)

(THRU)

55 (PAGES)

1 (CODE)

(NASA CR OR TMX OR AD NUMBER)

18 (CATEGORY)

GPO PRICE $

CSFTI PRICE(S) $

Hard copy (HC) 3.00

Microfiche (MF) .50

ff 653 July 65

AVCO CORPORATION
TULSA DIVISION

Rq/23238

FOREWORD

This report was prepared by the Avco Corporation/Tulsa Division as the final documentation of work performed under Contract NAS9-2939 issued by the National Aeronautics and Space Administration - Manned Spacecraft Center. This program was monitored by Dr. W. R. Downs of the Manned Spacecraft Center.

This report covers work performed from June, 1964 through June, 1965.

Prepared by: R. H. Jones
R. H. Jones
Staff Scientist

Approved by: M. I. Gamble
M. I. Gamble, Manager
Spaceflight Design Programs

Approved by: F. R. Riddell
F. R. Riddell
General Manager

TABLE OF CONTENTS

		Page No.
	Summary	1
I.	Introduction	2
II.	Nature of the Optical Degradation Mechanism	4
III.	The Space Radiation Environment	6
	A. The Solar Wind	6
	B. Solar Flare Radiation	6
	C. Auroral Protons and Electrons	8
	D. Trapped Protons and Electrons	8
	E. Galactic Cosmic Rays	9
	F. Micrometeoroids	10
	G. The Electromagnetic Spectrum	10
IV.	Analysis of the Significance of Space Radiation Components Toward Degradation to the Apollo Window	16
	A. Determination of the Most Damaging Components	16
	B. Summary of Worst Case Fluxes	17
V.	Selection of the Test Environment	19
VI.	Description of Equipment and Techniques	22
VII.	Results	26
VIII.	Conclusions	37
IX.	Appendix	39
	A. Ultra-High Vacuum System Description	39
	B. Radiation Source Description	43
	References	47

LIST OF FIGURES

Figure No.		Page No.
1	SPECTRA of Particles in Space	7
2	Extraterrestrial Solar Irradiance (Relative) According to F. S. Johnson	11
3	Solar Electromagnetic Radiation, at Earth's Distance from the Sun	14
4	Solar Spectral Energy Distribution from 2000 Angstroms to X-Rays	15
5	Spectral Transmittance of Corning No. 7940, Uncoated	28
6	Spectral Transmittance of Corning No. 7940, Coated (Outer Window)	29
7	Spectral Transmittance of Corning No. 1723, Coated (Inner Pane)	30
8	Spectral Transmittance of Owens-Illinois Inorganic Polymer No. 650	31
9	Spectral Transmittance of Owens-Illinois Inorganic Polymer No. 100	32
10	Spectral Transmittance of Stretched Plexiglass	33
11	Spectral Transmittance of Acrylic Sheet	34
12	Spectral Transmittance of Cross-Linked Methacrylate	35
13	Spectral Transmittance of Copolymer Styrene	36
14	Schematic of Ultra-High Vacuum System	40
15	Plan View of Space Simulation Facility	44

LIST OF TABLES

Table No.		Page No.
I	Materials Tested	2
II	Cumulative Extraterrestrial Energy Distribution of the Sun at 1 A. U. Distance	12
III	Intensity at 1 Astronomical Unit Produced by the Strongest Solar Emission Lines	13
IV	Near-Earth Space Radiations of Possible Significance to Optical Degradation of Apollo Window Materials (Worst Case)	18

SUMMARY

63370

Nine samples of prospective Apollo window materials were exposed to a simulated space radiation environment consisting of combined low energy protons (50 kev) and electromagnetic radiation, with wavelengths from 1216 angstroms in the extreme ultraviolet to two microns in the infrared. An accelerated two-week mission was simulated, assuming a solar flare to occur during the period. The purpose of the tests was to determine the optical degradation resulting from such exposure with the damage criterion being the observed change in spectral transmittance. Degradation was found to occur to varying degrees in all materials tested with Corning No. 7940 showing the least effect. Spectral transmittance curves of each material, made in situ, are presented for several increments of radiation dosage.

Author

I. INTRODUCTION

The terms of the above named contract with the National Aeronautics and Space Administration called for the determination of the effect of a 340 hour (approximately two weeks) Apollo mission on prospective window materials, with regard to optical degradation, as indicated by change in the spectral transmittance resulting from exposure to radiations simulating those expected during the planned mission. As a worst case it was assumed that a solar flare occurs.

The window materials supplied by the NASA were as follows:

Table I

MATERIALS TESTED

Material	Thickness	Coated
Corning No. 7940 fused silica	1/2 inch	No
Corning No. 7940 fused silica; coated (outer window)	11/16 inch	Yes
Corning No. 7940 fused silica; coated (outer window, aged)	11/16 inch	Yes
Corning No. 1723 aluminosilicate glass; coated (inner pane)	1/4 inch	Yes
Owens-Illinois No. 650 inorganic polymer	3/16 inch	No
Owens-Illinois No. 100 inorganic polymer	1/8 inch	No
Stretched plexiglass	1/4 inch	No
Acrylic sheet	1/4 inch	No.
Cross-linked methacrylate	1/4 inch	No
Copolymer styrene with divinyl benzene	5/16 inch	No
Corning No. 0311 "Chemcor"	1/8 inch	No

Since this work was initiated from the need to know the effects of radiation exposure on the visible portion of the spectrum, it was considered appropriate to investigate transmittance in the range extending from 0.45 microns to 0.73 microns. To eliminate the possibility that color centers formed during irradiation become bleached by time delay after cessation of an increment of flux or by exposure to air, it was considered necessary to conduct the transmittance measurements in situ with no disturbance to the test sample other than the temporary interruption of irradiation for 20 to 30 minutes.

Another prominent feature of the test program was the simultaneous exposure of the materials to the combined environment for determination of the synergistic effects. This required the use of a special triple entry port in which the protons, the solar beam and the extreme ultraviolet radiation were introduced along different paths so that all beams converged on the sample in the vacuum chamber, which was maintained at a pressure of 10^{-9} torr for samples such as quartz. The pressure was higher (10^{-7} torr) for some of the plastic materials which outgassed considerably, especially while being irradiated.

After selected increments of radiation exposure, the various radiation sources were interrupted long enough to make spectral transmittance measurements with a Perkin-Elmer Model 112U recording spectrophotometer. The light for the measurements was supplied by a tungsten source, the focused light from which was directed along the same path normally taken by the solar beam. The light then passed through the sample, out a sapphire exit window and into the spectrophotometer entrance slit. Spectral energy distribution of the source was recorded without the test sample in position, then again with the sample in the light beam before irradiation and after each accumulated dose of radiation. With this information the transmittance initially and at each stage of the irradiation process was calculated and plotted. Details of the experimental equipment and techniques will be discussed later.

II. NATURE OF THE OPTICAL DEGRADATION MECHANISM

Most of the information concerning damage to materials by nuclear radiations has come from nuclear energy studies and is based on gamma and neutron effects. Considerable data have been compiled regarding the changes in physical properties brought about by damage from these radiations. However, in the study described here, only the effects on the transmittance of materials is involved, and only this aspect will be considered.

While the radiations to which these samples were exposed were 50 kev protons and photons in the wavelength range 0.12 microns to 2.0 microns, much of the previous work by others (Ref. 1-17) has dealt with discolorations resulting from gamma and x-radiation (Ref. 4, 5, 6, 13, 15, 16). Gigas, Ewbank, and Gruber report (Ref. 3, 16) irradiation damage to glasses using 0.4 mev protons. The consensus of these studies is that ionizing radiation of all types are capable of producing discoloration of transparent materials to a greater or lesser degree depending on the energy of the radiation, total flux, and type of material. Kircher and Bowman (Ref. 16), quoting from the work of Sun and Kreidl (Ref. 1) state that below 5×10^4 ergs/gm (C) coloration begins in some glasses. Most are highly colored by 10^8 ergs/gm (C) and nearly all are saturated by 10^{12} ergs/gm (C). Continued irradiation beyond this dose was said to produce mechanical damage.

An explanation of the mechanism of radiation produced discoloration has been given for alkali halide crystals (Ref. 11); and though the situation with regard to glass is considered to be more complex, the same concept is assumed to be applicable. In the case of the alkali halide, the energetic bombarding particles release electrons from their equilibrium positions within the lattice, thus creating electron-hole pairs. Some of the electrons recombine with the holes and others become trapped at vacancies where there would normally exist a halide ion. The trapped electrons may have energy levels in the F-band, thus creating color or F-centers which are capable of absorbing electromagnetic radiation in the visible part of the spectrum. If two electrons are trapped at a halide ion vacancy, an F'-center is formed. Alternately, the hole produced by the bombarding particle may wander around and become trapped at an ion vacancy, again giving rise to an absorption center.

The addition of impurities to the glass sometimes brings about greater resistance to the discoloring effects of energetic radiation, cerium being a noteworthy example. This could result from the cerium ion

filling the aforementioned vacancies, thus avoiding formation of F-centers, possibly replacing them with absorption centers in parts of the spectrum other than the visible.

Bleaching of discolored glass can sometimes be brought about by heating (Ref. 16) and in some cases by the mere passage of time at room temperature. Bleaching also may be effected by re-irradiation at visible wavelengths. Complete removal of the discoloration has been produced in this manner (Ref. 10) for certain materials. Further comments on the discoloration mechanisms may be found in Refs. 1, 2, 4 and 16.

III. THE SPACE RADIATION ENVIRONMENT

Much has been said about the near-earth space environment (Refs. 2 - 4 and 19 - 42) with considerable data being by now well established. The picture that emerges indicates that the space radiations may be divided into several distinct categories; i. e., solar wind protons, solar flare protons, auroral protons and electrons, trapped (Van Allen) protons and electrons, galactic cosmic rays, micrometeoroids, which may be thought of as macroscopic uncharged particulate radiation, and the electromagnetic spectrum. Probably the most concise graphical presentation of the known facts about the particulate components is one due to R. Madey (Ref. 32) shown in Figure 1. Let us consider these radiations in greater detail.

A. Solar Wind

It has been determined by numerous measurements in satellites and space probes that the sun emits a more-or-less continuous stream of particles, mostly very low energy protons, during quiescent conditions, known as the solar wind; but information on the flux and energy of these protons is scarce. Jaffe and Rittenhouse (Ref.24) have estimated up to 10^9 protons/cm^2-sec. at earth orbital distances with energies less than 3 kev. Roberts (Ref. 2) gives a figure of 5×10^9 particles/cm^2-sec. at about 1.4 kev.

B. Solar Flare Radiation

A solar flare takes place on the sun when the magnetic field associated with a sunspot, which normally restricts the flow of hot gases, collapses and brings about the ejection of large volumes of highly ionized gases to the chromosphere. The result is a burst of high-energy particles which leave the sun permanently. The radiation, consisting mostly of protons but with some heavier nuclei, have energies from 20 mev to 500 mev or greater with flux during large 3+ solar flares to about 10^4 protons/cm^2-sec. These bursts typically last about one day (Refs. 2, 34, 35, 36) occurring about once per month (Ref. 2). There are also low-energy (1/2 to 20 kev) protons from flares with flux possibly to 10^{12} protons/cm^2-sec. (Ref. 2, 37). One to forty times this number of low energy electrons of energies from 1/4 to 10 e.v. may accompany the protons.

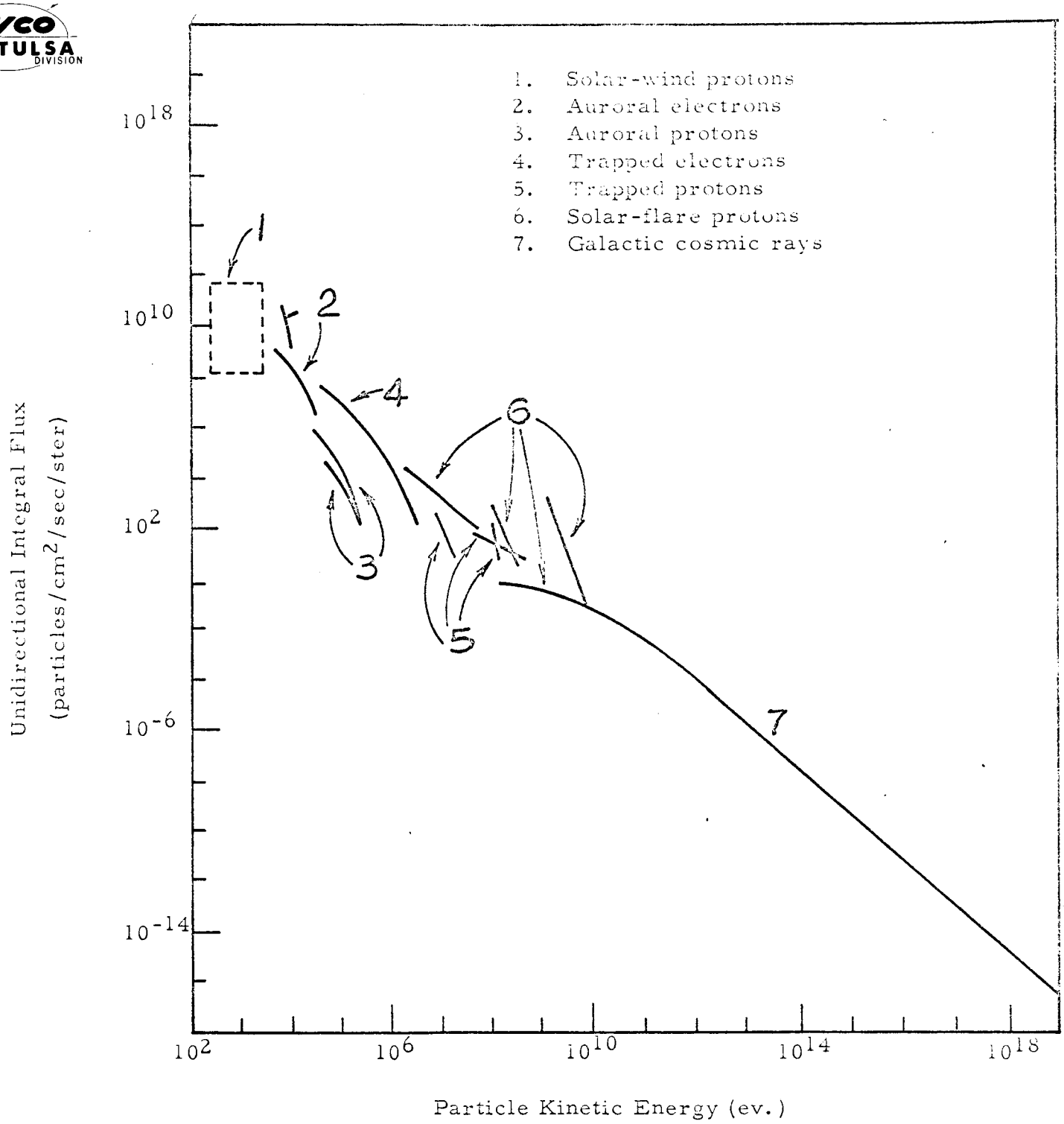

Figure 1 -- SPECTRA of Particles in Space (Ref. 32)

C. Auroral Protons and Electrons

Rockets have been flown into the auroral zones and have detected the presence of energetic protons and electrons. According to Dessler (Ref. 38), the proton flux above 100 kev lies generally between 10^5 protons/cm^2-sec and 10^6 protons/cm^2-sec. The electrons were nearly monoenergetic at around 6 kev (McIlwain, 1960). Other observations indicated 3 to 5 kev electrons with flux to 10^{10} electrons/cm^2-sec.

D. Trapped Protons and Electrons

The existence of two prominent bands of energetic trapped particles (Van Allen belts) is by now well known. These bands have approximately the shape of a torus in the equatorial plane compressed on the side of the earth toward the sun by the action of the electrically conductive solar wind on the earth's magnetic field, which also causes the belts to be elongated on the side of the earth away from the sun. The charged particles follow the magnetic lines, undergoing helical paths while oscillating back and forth between the northern and southern hemispheres. The radius of the helix diminishes as the particle decelerates when approaching either of the magnetic poles. There is still considerable question as to the origin of the trapped particles, but their flux distribution has been fairly well mapped (Refs. 2, 21, 26, 27, 28).

1. Inner Belt

In the equatorial plane the inner belt extends from about 400 km to 10,000 km (250 to 6000 miles) altitude. According to Jaffe and Rittenhouse (Ref. 2), the protons in the inner belt at its most intense region (3600 km or 2200 miles) range in energy from about one kev to 700 mev with integral fluxes of 10^8 protons/cm^2-sec and 10^2 protons/cm^2-sec, respectively. The fluxes below 7 mev were based on extrapolation of the energy spectrum between 80 and 450 mev. There were 3×10^{10} electrons/cm^2-sec of energy above 20 kev, 10^{10} electrons/cm^2-sec above 100 kev, and 10^7 electrons/cm^2-sec above 600 kev. Above one mev there were less than 10^5 electrons/cm^2-sec.

2. Outer Belt

The outer belt, extending from 10,000 km to 85,000 km (6,000 to 55,000 miles) altitude, has its most intense region at about 25,000 km (16,000 miles). Proton fluxes were estimated by Van Allen (Ref. 39) at 10^8 protons/cm^2-sec for energies between 0.1 mev and 5 mev. For energy above 30 mev the flux was 3×10^4 protons/cm^2-sec. Very energetic protons are practically non-existent in the outer belt, there being less than one proton/cm^2-sec above 75 mev. Electrons are very plentiful, the flux being 10^8 electrons/cm^2-sec for energies above 40 kev. A good discussion and graphical presentation of the facts pertaining to the constituents of the trapped radiation belts is given in an EOS report (Ref. 26, pp 2-1 through 2-34).

3. Artificial Belt

Mention should be made of the existence of a radiation belt of high-energy electrons, created by the high-altitude nuclear explosion (Starfish) over Johnston Island on July 9, 1962 and to a slight extent later by Russian tests. The first information after the explosion was compiled by Hess (Ref. 43) from data taken from then existing satellites, primarily Telstar I. He estimated a peak flux of about 1.6×10^9 electrons/cm^2-sec with energies to 7 mev. According to the estimate of McIlwain (Ref. 25), the lifetime may be long -- possibly ten years.

E. Galactic Cosmic Rays

Superimposed on the radiations mentioned heretofore is a background flux of high-energy particles emanating from beyond the solar system but whose intensity fluctuates inversely with solar activity. This is attributed to the effect of the solar magnetic field lines being carried further from the sun by bursts of particles from active solar regions, with resultant deflection of charged cosmic ray particles. The cosmic rays consist mostly of protons accompanied by a smaller number of alpha particles and a few heavier ions, electrons, and gamma rays. These primary cosmic rays should not be confused with the secondaries produced when they bombard the atomic nuclei in the earth's atmosphere. Energies range from a few mev to at least 10^6 bev with an average of 4 bev. An example of the flux is 0.77 particles/cm^2-sec for energies over 4.5 bev.

F. Micrometeoroids

These macroscopic particles of space dust are believed by some to originate from comets as is supposed for the visible meteors. Masses vary from 4×10^{-10} gm to 10^{-5} gm (Ref. 26) with velocities usually under 20 km/sec. According to Whipple (Ref. 40), the fluxes are extremely small, being about 10^{-8} impacts/m^2-sec for particles of mass greater than 10^{-5} gm.

G. The Electromagnetic Spectrum

The irradiance from the sun at a distance of one astronomical unit, called the solar constant, is 2.0 calories/cm^2-min (140 mw/cm^2) with 98.7 percent of the energy existing in the spectral range from 0.3 to 7.0 microns. In an orbit at 100 miles altitude, the effect of the earth's albedo is of importance in determining the total irradiance to which a satellite is exposed. However, for interplanetary travel in which the percentage of mission duration spent near earth is likely to be small, the effect of albedo is relatively unimportant. Sun spots and solar flares have a negligible effect on the solar irradiance, amounting to less than 0.4 percent change (Ref. 26). Several attempts have been made to estimate the solar spectral energy distribution, but the most generally referenced one is Johnson's (Ref. 41). Figure 2 shows his results as relative spectral irradiance vs. wavelength over that part of the spectrum containing the most appreciable intensities. Table II gives the cumulative energy distribution at various wavelengths, and Table III gives intensities of the strongest solar emission lines. In Figure 3, data from numerous investigators concerning the spectral irradiance is compiled (Ref. 2) for various portions of the spectrum, and Figure 4 shows a similar compilation for wavelengths from 2000 angstroms to x-rays (Ref. 42). It summarizes results of rocket measurements and gives data taken during a sunspot minimum in 1943-1954 labeled A-16, and during a sunspot maximum in 1956 labeled A-43. The extra curve added to A-16, marked 2×10^6, represents an increment of flux measured below 20 angstroms. The hydrogen Lyman alpha line is by far the strongest in the extreme ultraviolet (e.u.v.) region with an irradiance of 5.1 ergs/cm^2-sec.

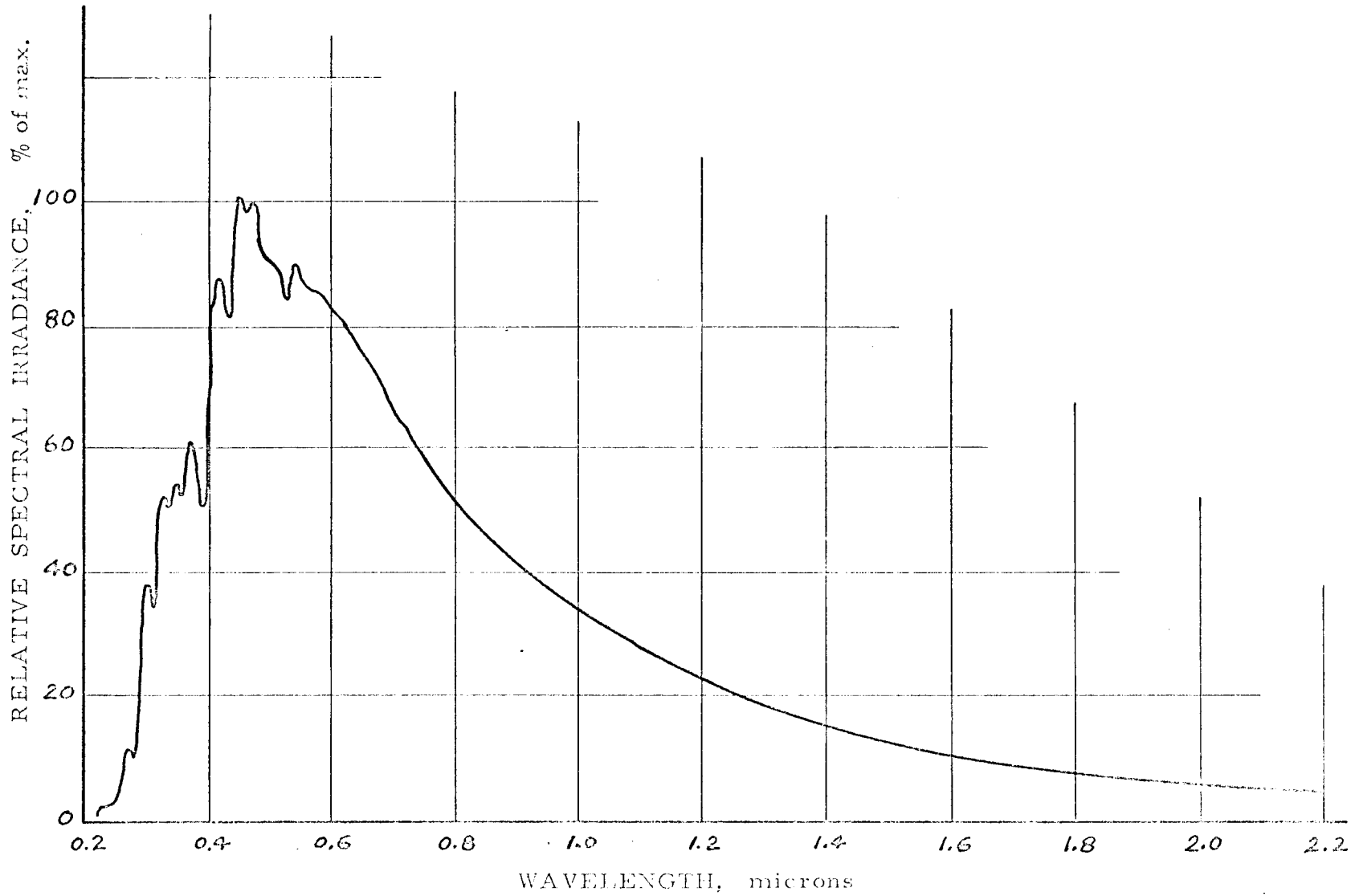

FIG. 2
EXTRATERRESTRIAL SOLAR IRRADIANCE
(RELATIVE)
ACCORDING TO F. S. JOHNSON

Table II

CUMULATIVE EXTRATERRESTRIAL ENERGY DISTRIBUTION OF THE SUN AT 1 A. U. DISTANCE (Ref. 2)[a]

Up to Wavelength, Å	Fraction of Total Energy	Energy, at Sunspot Maximum (including flares) erg/cm^2/yr
0.1	10^{-11}	$10^2 - 10^3$[b]
1	10^{-11}	$10^2 - 10^3$
10	10^{-8}	$10^5 - 10^6$
100	10^{-6}	$10^7 - 10^8$
500	10^{-6}	10^8
1,000	10^{-5}	10^8
1,500	10^{-5}	10^9
2,000	10^{-4}	4×10^9
2,500	1.3×10^{-3}	6×10^{10}
3,000	1.2×10^{-2}	5×10^{11}
4,000	9×10^{-2}	4.0×10^{12}
5,000	0.24	1.1×10^{13}
6,000	0.37	1.6×10^{13}
8,000	0.58	2.6×10^{13}
9,000	0.65	2.9×10^{13}
10,000	0.71	3.2×10^{13}
15,000	0.88	3.9×10^{13}
20,000	0.94	4.2×10^{13}
30,000	0.98	4.3×10^{13}
70,000	0.999	4.4×10^{13}

a. Data above 2000 Å from Johnson (Ref. 41).
b. 10^9 to 10^{10} photons/cm^2-yr. shorter than 0.1 Å.

Table III

INTENSITY AT 1 ASTRONOMICAL UNIT PRODUCED BY THE STRONGEST SOLAR EMISSION LINES (Ref. 42)

λ(Å)	Identification	Erg/cm^2/sec
1802.03	Si III (1)	0.10
1817.42*	Si II (1)	0.45
1808.01		0.15
1670.81	Al II (2)	0.08
1657.00*	C I (2)	0.16
1640.47	He II (12)	0.07
1561.40*	C I (3)	0.00
1550.77	C IV (1)	0.06
1548.19	C IV (1)	0.11
1533.44	Si II (2)	0.041
1526.70	Si II (2)	0.038
1402.73	Si IV (1)	0.013
1393.73	Si IV (1)	0.030
1335.68	C II (1)	0.050
1334.51	C II (1)	0.050
1306.02	O I (2)	0.025
1304.86	O I (2)	0.020
1302.17	O I (2)	0.013
1265.04	Si II (4)	0.020
1260.66*	Si II (4)	0.010
1242.78*	N V	0.003
1238.80	N V	0.004
1215.67	H Ly-α	5.1
1206.52	Si III (2)	0.030
1175.70*	C III (4)	0.010
1139.89*	C I (20-23)	0.003
1085.70*	N II (1)	0.006
1037.61*	O VI (1)	0.025
1031.91	O VI (1)	0.020
1025.72	H Ly-β	0.060
991.58*	N III (1)	0.010
989.79*	N III (1)	0.006
977.03	C III (1)	0.050
949.74	H Ly	0.010
937.80	H Ly	0.005
835*	O II, III	0.010

The value for Lyman-α applies to the intensity within the 1-Å wide central part of the line (based on an ion-chamber reading of 6.0 erg/cm^2/sec).

*Indicated that the line is a blend of lines of other elements or is an unresolved multiplet.

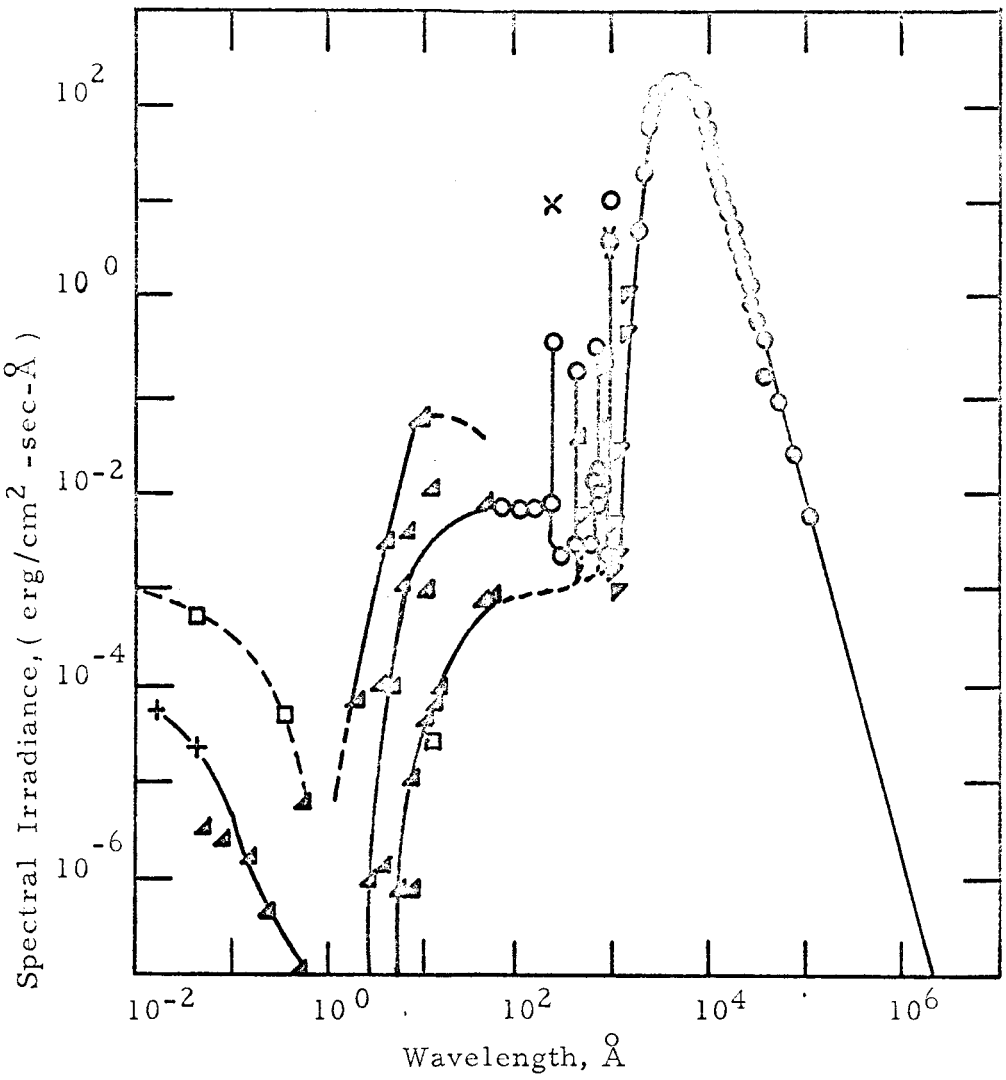

□ Peterson & Winckler et al
◢ Friedman et al
○ Hinteregger
◤ Tousey et al
⊙ Johnson
× Rense et al
+ Northrup & Hosteler

Legend

Figure 3
SOLAR ELECTROMAGNETIC RADIATION, AT EARTH'S DISTANCE FROM THE SUN

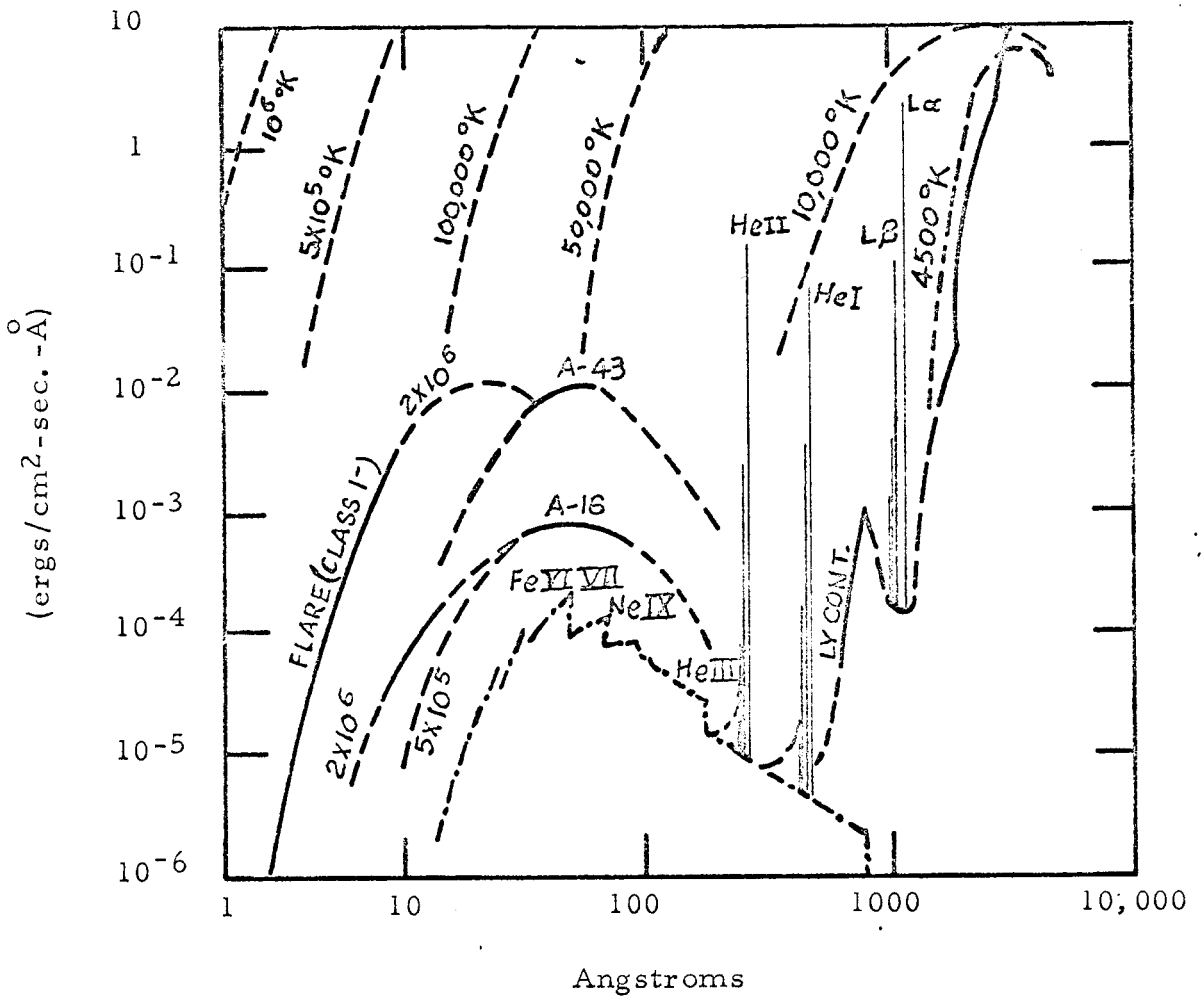

Figure 4 -- Solar Spectral Energy Distribution from 2000 Å to X-Rays

IV. ANALYSIS OF THE SIGNIFICANCE OF SPACE RADIATION COMPONENTS TOWARD DEGRADATION TO THE APOLLO WINDOW

A. Determination of the Most Damaging Components

In consideration of the facts brought out in the previous sections, it may be concluded that the radiations present in extraterrestrial space which are likely to cause degradation of optical windows are the u. v. and e. u. v. portion of the electromagnetic spectrum, the solar wind protons, the solar flare protons and electrons, and the trapped protons and electrons.

1. The Solar Electromagnetic Spectrum

In Section II, it was brought out that exposure to visible light of a glass sample which has been previously discolored by more energetic radiations often results in partial or complete bleaching. This suggests the importance of testing for degradation with simulated solar radiation covering as much of the spectrum as is possible because, even though the energetic ultraviolet may produce degradation, the longer visible and infrared waves may synergistically destroy the F-centers, resulting in little or no observable discoloration.

2. Solar Wind and Flare Particles

Regarding the particulate radiations of space, the low energy protons comprising the solar wind (10^9 to 5×10^9 protons/cm^2-sec) are vastly in excess of all others except for the protons and electrons during a solar flare when the low energy flux, it will be recalled, is possibly as high as 10^{12} protons/cm^2-sec with one to 40 times as many electrons with energies less than 10 ev. For a 340 hour (1.22×10^6 sec) mission and considering the worst case, the total number of solar wind protons encountered is 5×10^9 protons/cm^2-sec $\times$ 1.22 sec = 6.1×10^{15} protons/cm^2. If a one-day (8.65×10^4 sec) flare occurs, the window receives 10^{12} protons/cm^2-sec $\times$ 8.65×10^4 sec = 8.7×10^{16} protons/cm^2 and possibly as high as 35×10^{17} electrons/cm^2.

3. Trapped Particles

The trapped radiation belts comprise the next most significant possible source of damage to window materials. Without

performing an integration of the differential flux to the window while moving through the trapped particles along the planned Apollo flight path, it is difficult to estimate the total number of particles striking the window. Although the high energy particles will be detrimental to the glass, their effect will be relatively insignificant compared to that of the low energy components because of their vastly lower numbers.

The high energy particles, some of which may penetrate the vehicle and can also produce energetic bremsstrahlung, will be the greater hazard to the astronauts. As a worst case, using 10^8 protons/cm^2-sec and 3×10^{10} electrons/cm^2-sec, and assuming the vehicle to remain in the belts for 5 hours (1.8×10^4 sec), the window would encounter 1.8×10^{12} protons/cm^2 and 5.4×10^{14} electrons/cm^2. These figures, though possibly unrealistically high, are still much below the contributions from the solar wind and flare.

Regarding the trapped electrons in the artificial belt, using the flux given by Hess of 1.6×10^9 electrons/cm^2-sec of energies to 7 mev (assuming the belt still to be active at the time of the Apollo mission) with exposure for five hours, the window would encounter 2.9×10^{13} electrons/cm^2.

4. Aurora and Galactic Cosmic Rays

The remaining space radiations from the aurora (which will not be encountered near the equatorial plane, as in the case of the Apollo mission) and galactic cosmic rays are so low in flux as to be negligible.

B. Summary of Worst Case Fluxes

In summary, the worst case contributions of solar wind, solar flare, and trapped particles to the radiation environment relevant to the testing of Apollo window materials are as shown in Table IV on the following page.

Table IV

NEAR-EARTH SPACE RADIATIONS OF POSSIBLE SIGNIFICANCE TO OPTICAL DEGRADATION OF APOLLO WINDOW MATERIALS (WORST CASE)

Particle	Source	Energy	Particles/cm^2 Encountered by Window during Mission
Protons	Solar Wind	1 to 3 kev	6.1×10^{15}
Protons	Solar Flare	1/2 to 20 kev	8.7×10^{16}
Protons	Trapped (Natural)	Near 1 kev	1.8×10^{12}
Electrons	Solar Flare	1/4 to 10 ev.	35×10^{17}
Electrons	Trapped (Natural)	20 to 600 kev	5.4×10^{14}
Electrons	Trapped (Artificial)	Less than 7 mev	2.9×10^{13}

V. SELECTION OF THE TEST ENVIRONMENT

Considering the time limitation imposed by the period of the contract and the complexity of the space environment, it was necessary to reduce the simulated space parameters to the smallest number consistent with the need for reaching meaningful conclusions of probable validity. It would be desirable to find the degradation as a function of all of the significant parameters; i. e., type of window material, type of radiation, energy of radiation, radiation dose, temperature, etc., and to perform the tests synergistically except for the variation of the parameter being investigated at a particular time. In addition, it would be desirable to simulate in real time so that rate effects may be ruled out. Consideration of these problems reveals that the practical time limitation would be vastly exceeded.

To measure synergistic radiation effects as a "function" of each important parameter means that only one particular parameter is varied at a time, the remaining ones being held stationary. Also, to find even the most approximate functional relationship, several (assume four) points on a curve are needed. Of the parameters mentioned above, the only one not requiring that a new (exactly identical) sample be used for each datum point on the curve of a particular function is the radiation dose. Otherwise a new sample, each requiring 340 hours (2 weeks) of test time, would have to be inserted for each of the literally thousands of combinations of parameters needed to obtain all the desired information. It is true that with ingeneous programming of the tests, the need for many combinations can be eliminated, but the time and quantity of samples required is at best formidable.

Considering the above difficulties in obtaining the desired information from a program of this type, it is clear that the tests must be limited to a relatively small number. Therefore, those radiations were chosen from Table IV whose effects were considered to be the most appreciable. This approach led to the selection of the protons since electrons in comparable numbers coming from solar flares have very low energies (less than 10 ev.) and would not be expected to be as damaging as the protons.

Considerable difficulty was encountered before a reliable source of e. u. v. was developed. The original source was found to exhibit spurious glow discharges off the optical axis which could not be seen

from the sample position and subtracted from the usable e. u. v. output. This problem consumed enough time to aggravate the need for maximum irradiation time. In view of this situation, a test schedule was chosen in which each type of Apollo window material was exposed to the following environment:

1. Vacuum: 10^{-7} to 10^{-9} torr (10^{-7} for outgassing plastic materials, usually 10^{-9} for others).

2. Temperature: Sample holder liquid cooled at room temperature.

3. Particulate Radiation: 50 kev protons, 10^{17} protons/cm^2 total at flux rate of 1.57×10^{12} protons/cm^2-sec.

4. Electromagnetic Radiation: Simulated solar (Johnson) spectrum at 7-1/2 suns. Also, simulated solar e. u. v. spectrum at 7-1/2 suns produced by a hydrogen discharge.

5. Time Simulated in Space: 340 hours (45 hours real time).

The transmittance of the samples was measured *in situ* before irradiation and immediately after each of the following total exposures:

1. 10^{16} protons/cm^2 and 14 sun-hours of electromagnetic radiation.

2. 10^{17} protons/cm^2 and 170 sun-hours of electromagnetic radiation.

3. 10^{17} protons/cm^2 and 340 sun-hours of electromagnetic radiation.

The materials listed below were tested:

1. Corning No. 7940 fused silica, 1/2 inch thick.

2. Corning No. 7940, coated (outer window), 11/16 inch thick.

3. Corning No. 1723, coated (inner pane), 1/4 inch thick.

4. Owens-Illinois No. 650 inorganic polymer, 3/16 inch thick.

5. Owens-Illinois No. 100 inorganic polymer, 1/8 inch thick.

6. Stretched plexiglass, 1/4 inch thick.

7. Acrylic sheet, 1/4 inch thick.

8. Cross-linked methacrylate, 1/4 inch thick.

9. Copolymer styrene with divinyl benzene, 5/16 inch thick.

The choice of these conditions was a compromise between various opposing factors. First, it may be said that accelerated, rather than real time, testing was necessary in order to test the maximum number of samples in the allowable time; however, the degree to which the flux rates could be increased was limited by the capabilities of the equipment and the danger of rate effects in the sample materials. The total proton dose was applied faster than was the electromagnetic radiation. Two factors contributed to this situation: one was that it was important to have someone in attendance of the Van de Graaff accelerator at all times during its operation. This would have required 24-hour shift work, so to avoid interrupting the irradiation, which could allow bleaching of a possibly discolored sample, the proton flux was increased. The other factor was that because these tests included the simulation of a solar flare, an increase of proton flux rate relative to the elctromagnetic was considered appropriate.

The use of 50 kev protons was brought about by the difficulty of achieving the needed flux rates at lower energy. It is believed that simulating the total flux encountered in space has greater bearing on glass degradation than has the particular energy of the particle doing the damage.

VI. DESCRIPTION OF EQUIPMENT AND TECHNIQUES

The heart of the simulation facility (see Figure 15 in the Appendix) is the vacuum chamber in which the sample is placed for irradiation. It is essentially a stainless steel cylinder with associated roughing, titanium sublimation, and sputter ion pumps. The proton radiation is fed to the vacuum chamber through an entry port so constructed as to introduce the beam via a tube directed at the sample, which is mounted near the center of the chamber. The entry port contains another tube through which the e. u. v. radiation from a hydrogen discharge source enters. The tube is mounted below and to the side of the proton line in a plane which intersects the proton beam at the sample position. The special entry port also contains a quartz window through which the beam from the solar simulator enters at a 90 degree angle to the proton beam. An aluminized, first surface mirror is mounted inside the entry port at a 45 degree angle and in a position such that the beam is directed onto the sample without interfering with the proton and e. u. v. beams. The protons are supplied by a Van de Graaff accelerator (0.5 mev max.). Its beam is fed through an analyzing magnet for separating the protons from the other hydrogen isotopes (and any impurities which may be present in the hydrogen source) and from there the protons pass through a pair of orifices. Their purpose is to permit the test chamber to be kept at a high vacuum (10^{-9} torr to 3×10^{-10} torr) while the proton accelerator tube remains at around 10^{-5} torr. This is accomplished by pumping the space between the orifices to a lower pressure than exists in the accelerator tube, made possible by the limited conductance of the orifices. The proton beam, after passing through, emerges as a ribbon of particles, since the orifices are actually slits. The protons then pass between two electrostatic deflection plates to which is applied an oscillating voltage of sawtooth waveform. This rasters the beam which scans back and forth across the test specimen, spending an equal percentage of each cycle on all exposed parts of the specimen. This is the technique used to provide uniformity of exposure.

The extreme ultraviolet portion of the spectrum was simulated by a liquid cooled hydrogen discharge source utilizing the Penning geometry. One of the electrodes is slotted to permit the e. u. v. radiation, consisting of the hydrogen spectrum, to escape from the region of ionization. The source is provided with a lithium fluoride window to pass as much as possible of the e. u. v., containing a continuum and the strong Lyman alpha line. The source is flange mounted to the e. u. v. tube on the triple entry port.

Calibration of the e. u. v. source was done by using as a standard a pre-calibrated nitric oxide ionization cell, obtained from GBL Associates. A ring shaped nickel photoelectric pickup probe mounted so as to intercept some of the e. u. v. getting to the sample was used to monitor the beam to check for constancy of output.

The portion of the spectrum from 0.2 microns to 2.0 microns was simulated by a single xenon lamp simulator made by Aerospace Controls Corporation. The use of G. E. 101 quartz for the beam forming lenses and Bausch & Lomb 90-8 reflective coating on the collector mirror shape the spectrum to approximate the Johnson spectrum. The beam from the solar simulator is directed into the quartz window of the triple entry port. Its radiation then impinges upon the test specimen.

The solar simulator was calibrated against an Eppley Mark III filter radiometer. However, since the Eppley radiometer is too large to pass through any of the several ports on the test chamber, it was necessary to use a small thermocouple radiometer which could be placed in the chamber. It was made by AVCO/Tulsa and calibrated against the Eppley Mark III. The AVCO radiometer consists of two thermocouples connected series opposing and mounted in a case in such a way that one of the junctions is exposed to the solar beam while the other is shielded from it. In this way, the ambient temperature cancels out but not the effect of the solar beam. Both junctions have spot welded to them identically sized silver discs, blackened with Parson's optical black lacquer. The shielded disc is exposed to the surrounding space through a hole in the side of the case. This feature equalizes the exchange of radiation of each disc with the ambient environment.

The sample holder consists of a square stainless steel block having a hole with a shoulder for mounting the test sample, which is held in position by four spring-loaded clamps at the edge. The holder has channels for circulation of cooling or temperature controlling liquid and is physically held in position near the center of the chamber by the tubes which carry the cooling liquid. They in turn are supported by the flange through which they enter the chamber. The temperature of the sample is measured with a thermocouple located at the rear edge so as not to be exposed to the solar beam. A copper disc to which the thermocouple junction is silver brazed is spring-loaded against the sample and the leads pass through the flange which supports the sample holder.

The proton beam current is picked up for measurement by use of an extremely fine tungsten screen held against the test sample. It is attached to the end of an open metal cylinder which is mounted in the sample holder, being insulated from it by a glass sleeve. The protons pass through the cylinder and screen before striking the test specimen. The charge which builds upon the specimen leaks to the screen and a wire connected to the cylinder conducts the current away for measurement. The screen, though it shields the sample from some of the protons, causes negligible error because its area is less than 1% of the exposed area of the sample.

When protons strike the beam current pickup screen some secondary electrons are ejected. If these electrons are allowed to escape to the surroundings in the chamber, the beam current reading will be erroneously high. To avoid this, a 90-volt battery is connected in series with the beam current meter so that the pickup screen is biased positive, thus attracting the secondary electrons back and preventing their escape. An insulated metal plate with a hole in it for the passage of the protons is mounted just ahead of the sample holder and is similarly biased 90-volts positive with respect to ground. Its purpose is to define the area over which protons are delivered to the sample.

The transmittance measurements were made with a Perkin-Elmer Model 112-U recording spectrophotometer. It utilizes a single-beam double-pass prism monochromator, Model 99. In order to more adequately cover the long wavelength end of the visible spectrum, the 1P28 photomultiplier tube having an S-5 response was replaced with an RCA 7265 having an S-20 response.

The spectrum for the in situ measurements was supplied by a tungsten source mounted next to the triple entry port. A movable mirror made it possible to introduce either the solar beam or the light from the tungsten source into the quartz entry window. This was done by using a rotatable disc with an eccentric hole through one side and a mirror on the opposite side, the disc being mounted in the path of the solar beam. The solar beam enters the quartz window through the hole; or, by turning the disc 180 degrees, the solar beam is cut off and the light from the tungsten source is reflected into the path normally taken by the solar beam. From there it passes through the test sample, out of the chamber through a small sapphire exit window and comes to a focus just a few inches beyond that point where the monochromator entrance slit is positioned.

Once the sample is placed in the chamber, the incident spectrum can no longer be seen by the spectrophotometer, so special techniques are required to insure that the initial spectral measurements of the source remain valid as a reference for all successive measurements on a test sample. If the amplifier gain or the tungsten source intensity changed during a sample irradiation, these changes would appear to be due to change of transmittance of the test specimen. To avoid this difficulty, two steps were taken: one was to monitor the intensity of the spectrum source directly with a silicon cell placed inside the lamp housing. This revealed any change in lamp intensity during the test period. The other was the use of a small reference light source which could be placed precisely at the monochromator entrance slit. The reference source intensity was also monitored with a silicon cell placed inside its case. The use of this source revealed any change in the sensitivity of the spectrophotometer during the course of the tests. These precautionary measures made it possible to use the pre-irradiation spectral measurement of the light incident on the test sample as a valid reference with which to compare subsequent post-irradiation spectral measurements.

The inaccessibility of the incident light after placing a test specimen in the holder also made it necessary to compute the transmittances from the recorded spectral curves, rather than being able to set the spectrophotometer gain at each wavelength so that the incident light could be made to indicate 100 percent on the recorder. This means that the accuracy near the edges of the recorded spectrum is lower because the readings from the spectral curves are always low at those wavelengths. Noise measurements made on the system during operation showed that over the wavelength range used for these transmittance measurements, the error varied over the spectrum, being about $\pm$ 3% at 0.45 micron, $\pm$ 1.5% at 0.6 micron and $\pm$ 5% at 0.73 micron.

Additional information concerning the AVCO/Tulsa space simulation facility is given in the Appendix.

VII. RESULTS

The transmittance curves for the materials tested are given in Figures 5 - 13. The wavy appearance of the curves for the outer window and inner-pane is assumed to be due to interference bands produced by the coatings on these materials. The curves were derived as follows:

1. The spectrum of the tungsten source was scanned, using the spectrometer motor drive, and recorded before the sample was inserted.

2. The sample was then placed in the beam from the tungsten source at a point outside the test chamber and just ahead of the monochromator entrance slit. The spectrum was scanned and recorded again.

3. Light values read from the second curve were ratioed to those from the first and plotted at 0.1 micron increments. This gave the initial spectral transmittances shown on the graphs.

4. The sample was then placed in its holder inside the chamber and another spectrum was recorded after evacuating the chamber.

5. After the first dose of simulated space radiation was applied to the sample, another spectrum was recorded. Values from this curve were ratioed to those from the previous curve (step 4) and the resulting ratios multiplied by the initial transmittances. This gave the transmittance after the first dose.

6. After each additional dose, step 5 was repeated, resulting in the transmittance shown in Figures 5 - 13.

The plastic materials were degraded considerably more than the quartz, some to the point of charring. This was particularly evident in the case of stretched plexiglass, acrylic sheet, cross-linked methacrylate, and copolymer styrene. The Owens-Illinois inorganic polymer No. 100 charred and cracked during irradiation. The tungsten screen stuck to the sample of stretched plexiglass. These occurrences are assumed to have resulted from the high radiation flux densities necessary when using accelerated testing to reduce testing times to practical values. It is believed that once the darkening of the sample by the radiations (probably the protons) has begun, increased absorption of the simulated

solar energy heats the sample. Due to the poor thermal conductivity of the sample, the liquid-cooled holder is unable to remove the heat produced at the surface rapidly enough to prevent eventual charring. The more the sample darkens from the heating, the hotter it gets, so that the destruction is regenerative. The glasses do not char, so they survive the tests without this secondary degradation.

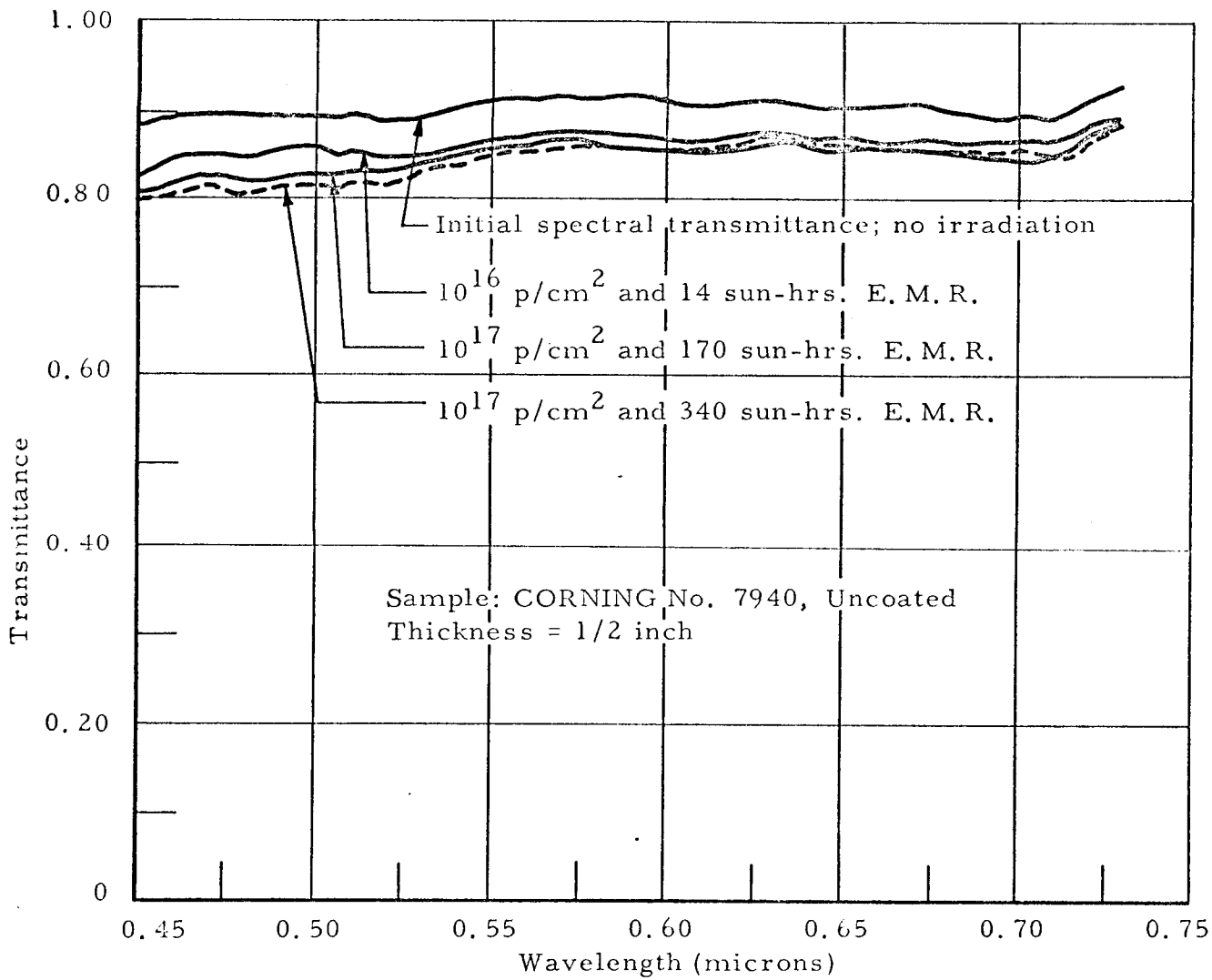

FIG. 5 THE EFFECT OF SIMULATED SPACE RADIATION ON THE TRANSMITTANCE OF PROSPECTIVE APOLLO WINDOW MATERIALS

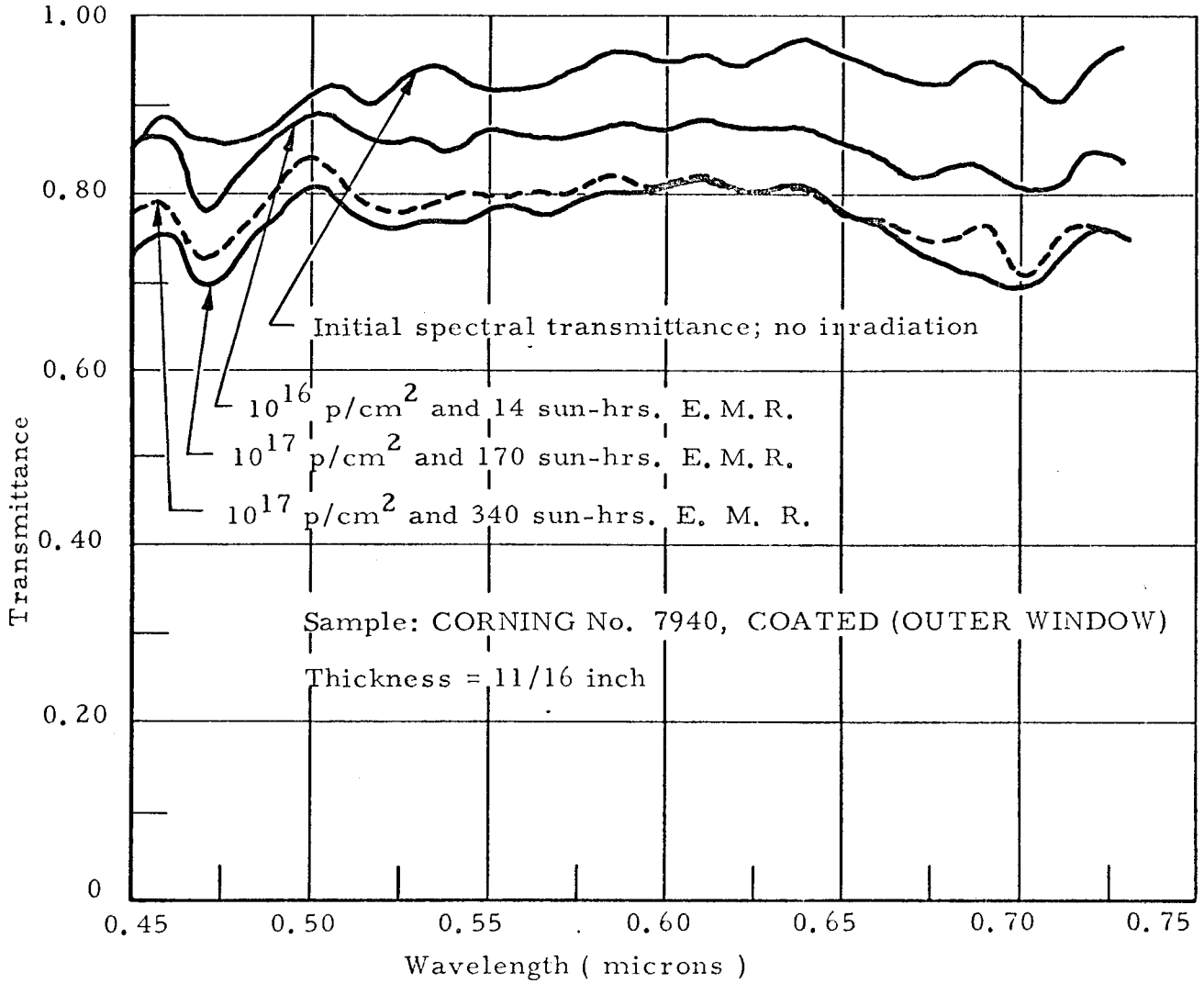

FIG. 6 THE EFFECT OF SIMULATED SPACE RADIATION ON THE TRANSMITTANCE OF PROSPECTIVE APOLLO WINDOW MATERIALS

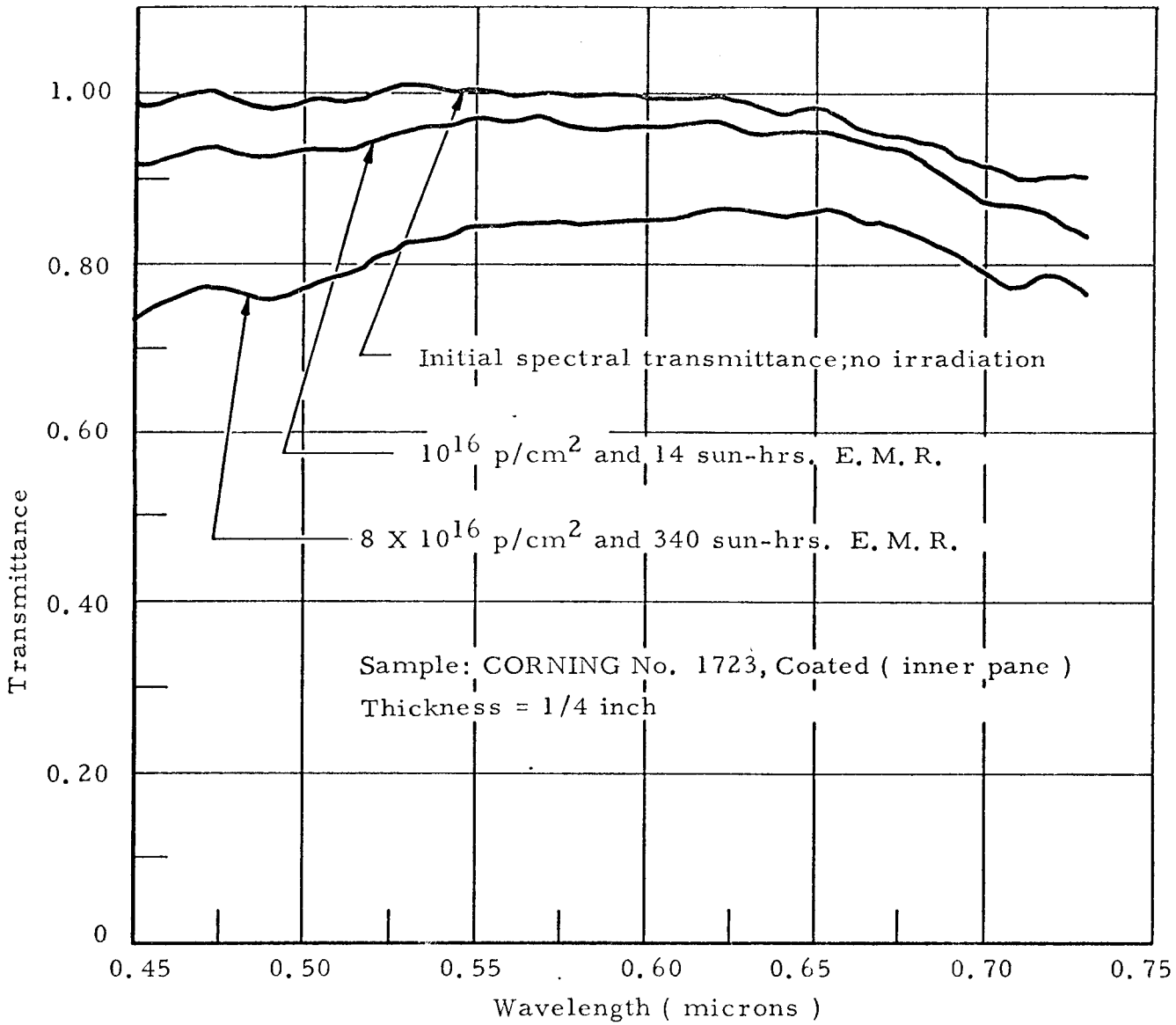

FIG. 7 THE EFFECT OF SIMULATED SPACE RADIATION ON THE TRANSMITTANCE OF PROSPECTIVE APOLLO WINDOW MATERIALS

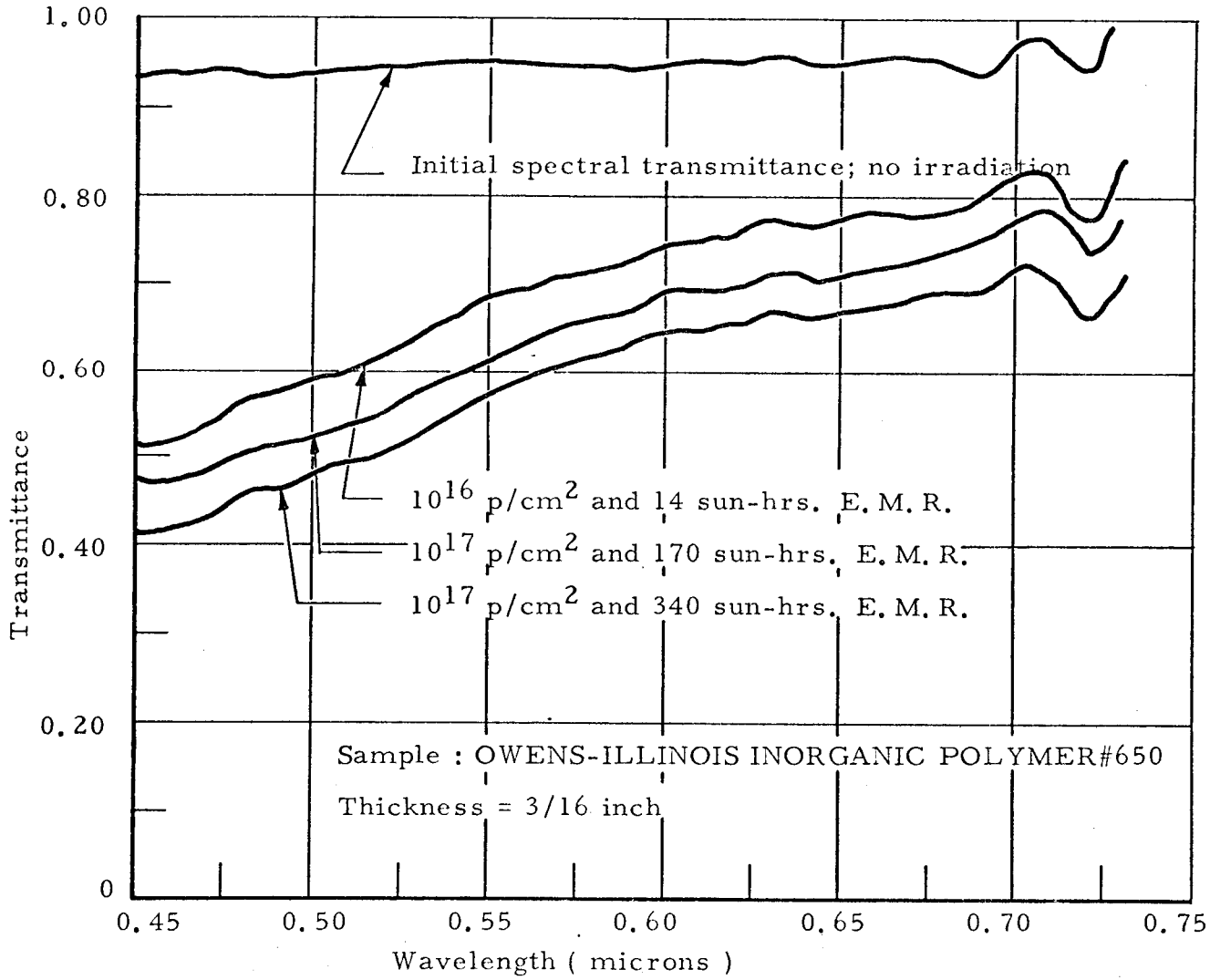

FIG. 8 THE EFFECT OF SIMULATED SPACE RADIATION ON THE TRANSMITTANCE OF PROSPECTIVE APOLLO WINDOW MATERIALS

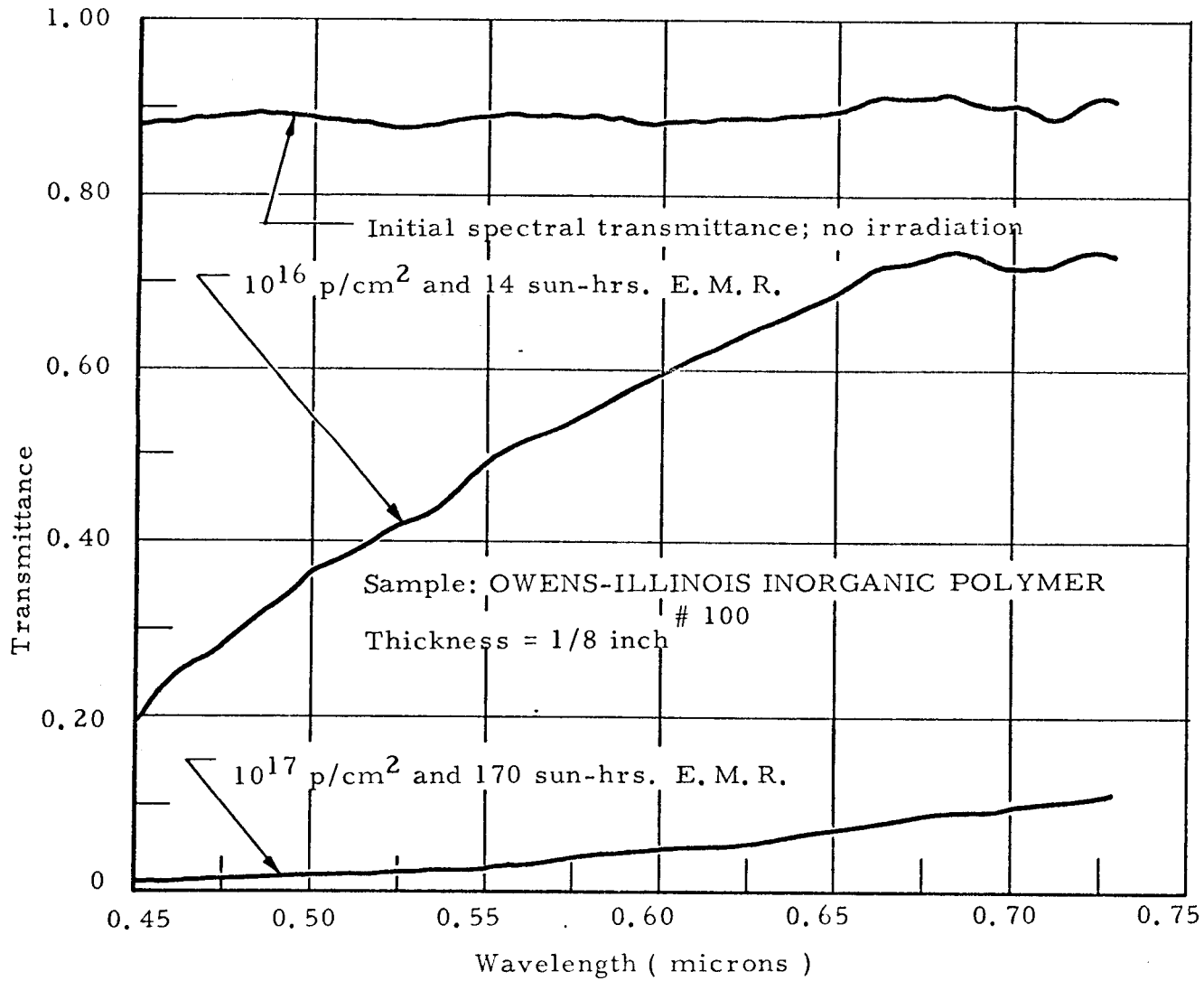

FIG. 9 THE EFFECT OF SIMULATED SPACE RADIATION ON THE TRANSMITTANCE OF PROSPECTIVE APOLLO WINDOW MATERIALS

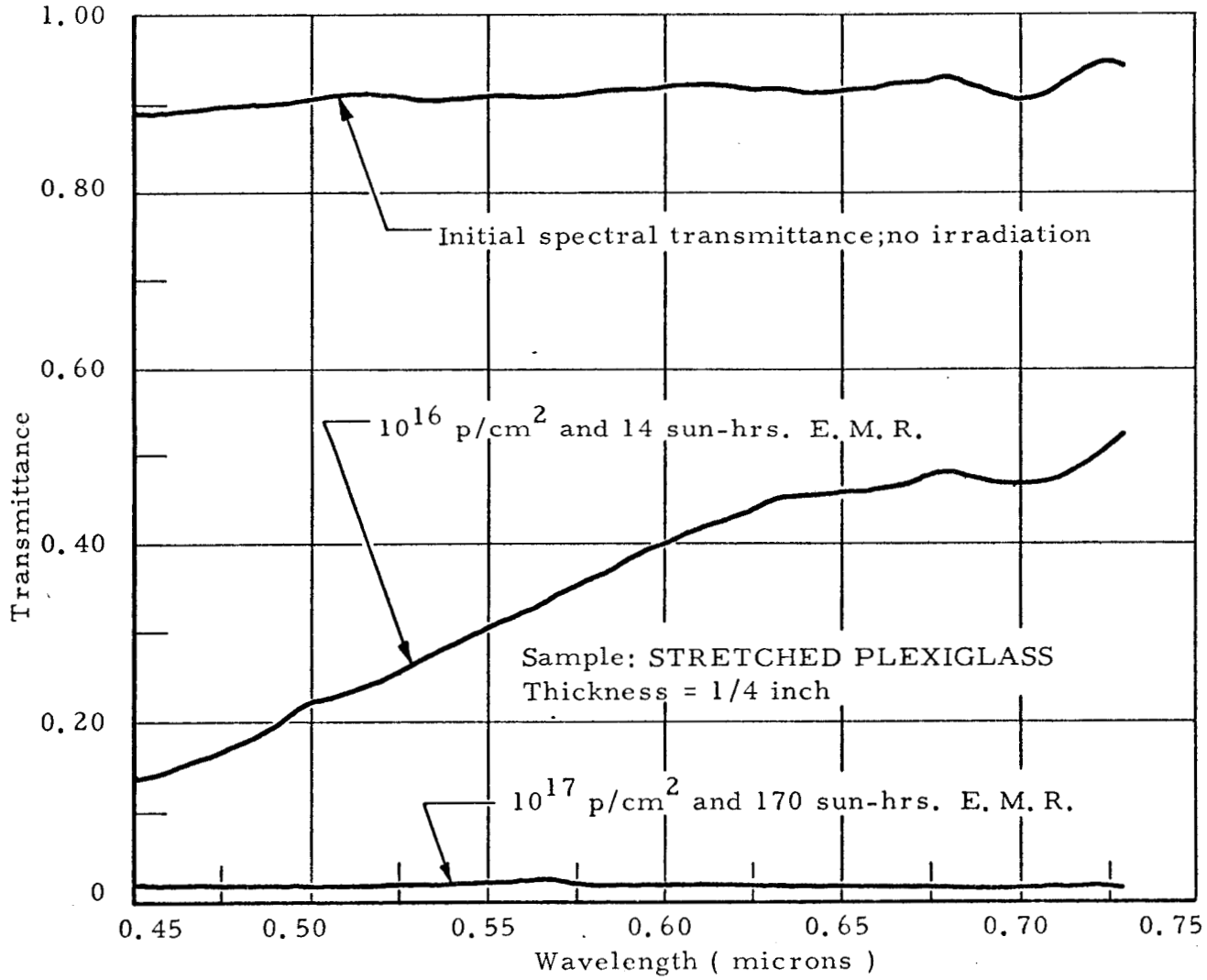

FIG. 10 THE EFFECT OF SIMULATED SPACE RADIATION ON THE TRANSMITTANCE OF PROSPECTIVE APOLLO WINDOW MATERIALS

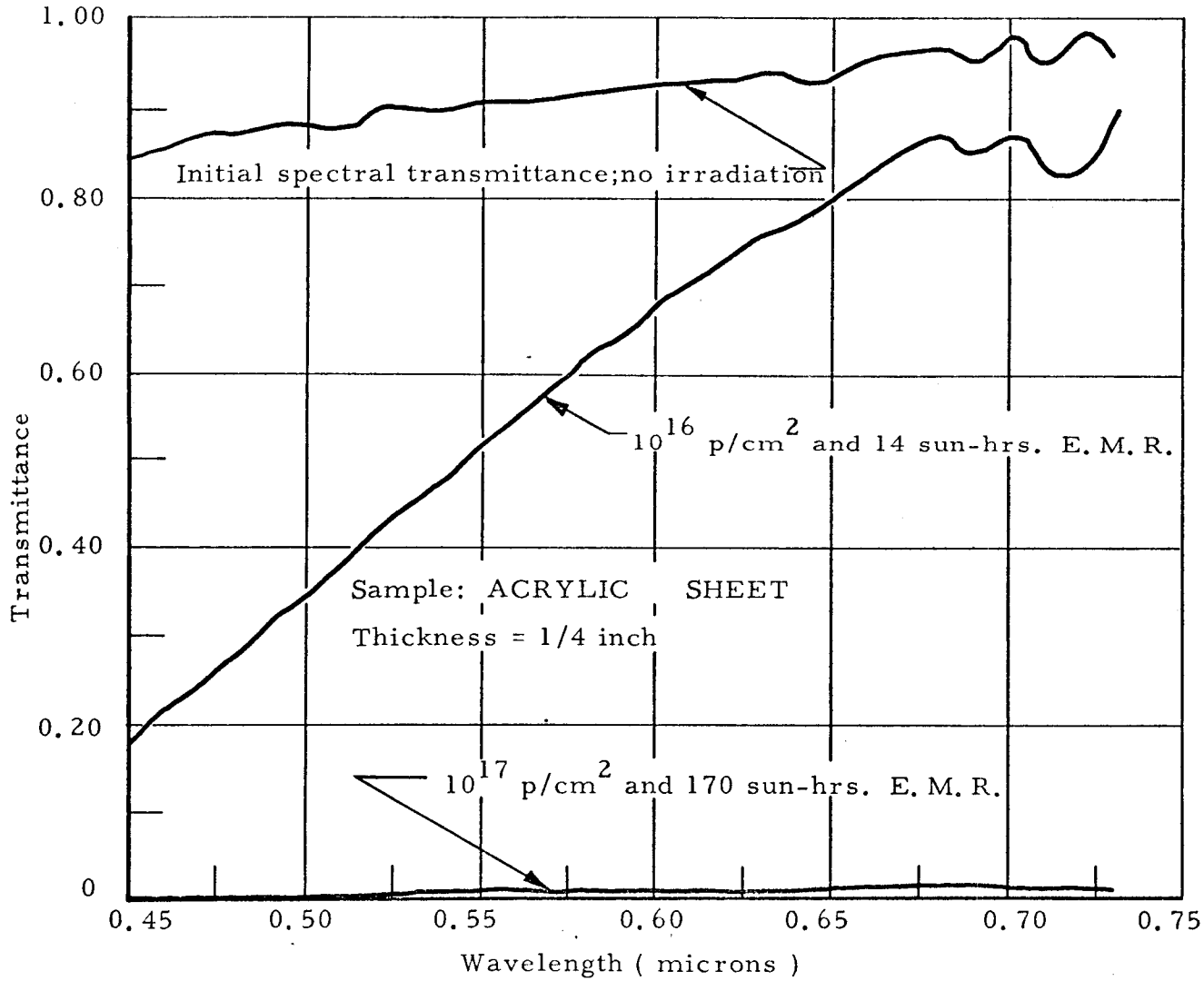

FIG. 11 THE EFFECT OF SIMULATED SPACE RADIATION ON THE TRANSMITTANCE OF PROSPECTIVE APOLLO WINDOW MATERIALS

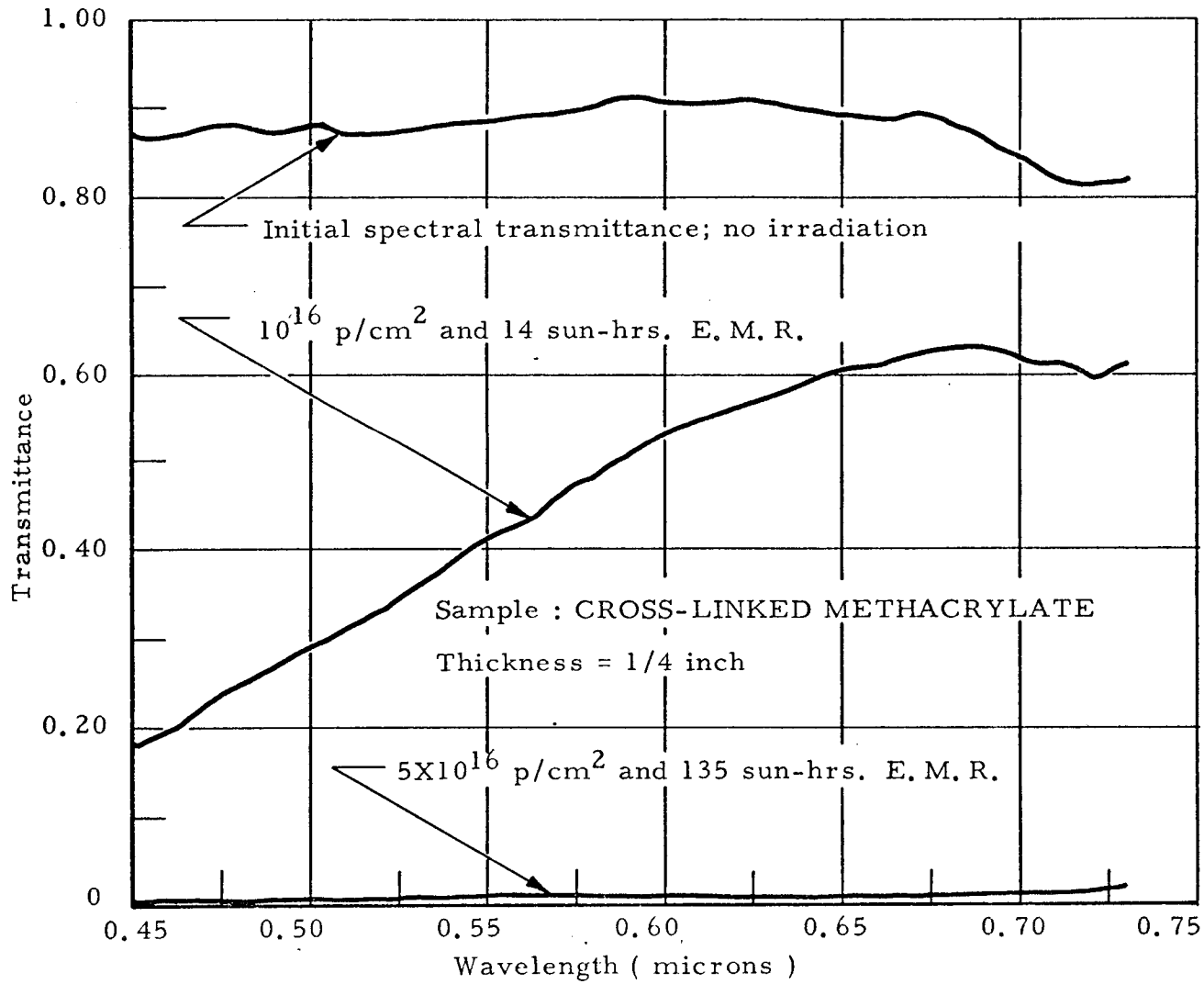

FIG. 12 THE EFFECT OF SIMULATED SPACE RADIATION ON THE TRANSMITTANCE OF PROSPECTIVE APOLLO WINDOW MATERIALS

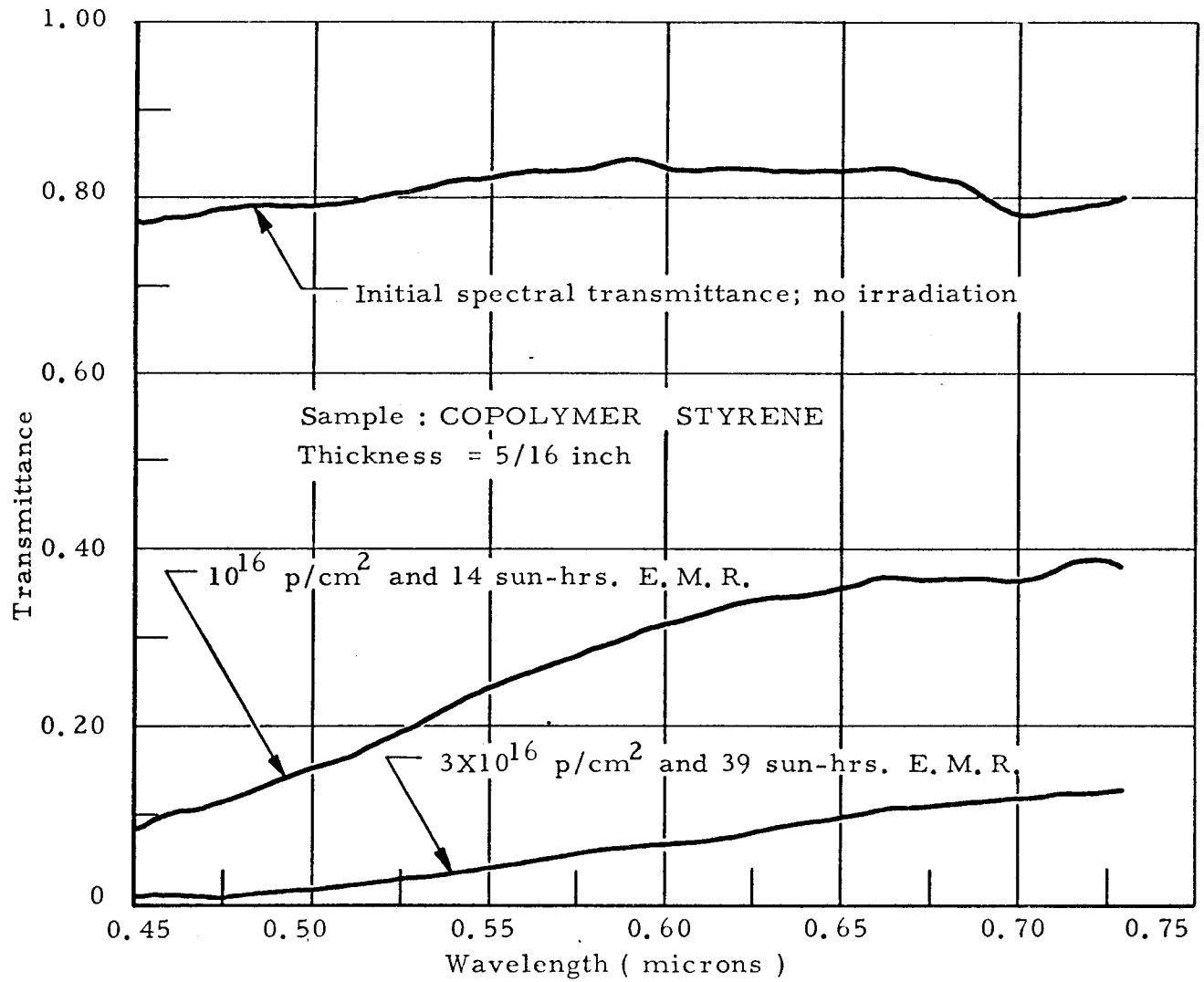

FIG. 13 THE EFFECT OF SIMULATED SPACE RADIATION ON THE TRANSMITTANCE OF PROSPECTIVE APOLLO WINDOW MATERIALS

VIII. CONCLUSIONS

The results clearly indicate that of the materials tested, uncoated Corning No. 7940 was the most radiation resistant, showing a decrease in transmittance of approximately five percent at 0.6 micron, near the middle of the visible spectrum. As is typical for most materials, the degradation was larger at the short wavelengths, less at the long wavelengths, with transmittance decreases of eight percent and four percent, respectively under exposure to 10^{17} protons/cm^2 (at 50 kev energy) and 340 sun-hours of electromagnetic radiation simulating the solar spectrum from 0.105 micron to over 2.0 microns.

Coated Corning No. 7940 showed somewhat more degradation, with 13 percent loss of transmittance at 0.6 micron. Unlike most materials, loss of transmittance was slightly less at the short wavelengths than at the long. In both the uncoated and the coated Corning No. 7940, the curves show that the transmittance changes were negligible during the last increment of irradiation, suggesting that the degradation to these materials was due to the protons. Unfortunately, a similar check could not be made for Corning No. 1723 (inner pane) because trouble with the equipment prevented the recording of a spectral curve after 10^{17} protons/cm^2 and 170 sun-hours of electromagnetic radiation (E.M.R.) as with the other materials.

Corning No. 1723 aluminosilicate glass, which changed significantly during the irradiation, still had reasonably high transmittance at the end of the test due to its very high initial transmittance (about 99%).

Following these in radiation resistance was Owens-Illinois No. 650 inorganic polymer which dropped in transmittance from 0.95 to 0.64 at 0.6 micron, a change of 33 percent.

All of the plastics tested degraded to near opacity. As mentioned previously, this is probably due in part to the heating which resulted from accelerated testing. However, it is believed that the results do indicate poor radiation resistance of these materials, based on the assumption that regenerative destruction would not begin unless significant degradation, not dependent on a rate effect, had taken place first. After the initial degradation, absorption of the simulated solar energy heats the sample, producing more discoloration, absorbing more energy, etc.

By bracketing the radiation doses required to degrade the more resistant materials, some insight has been gained into the likelihood of degradation on an Apollo mission. It may be said that for the most resistant material, Corning No. 7940, degradation is small under the worst suspected conditions. Even if the doses given in these tests are higher than would be encountered during an actual mission, the material appears to be a good prospect as an Apollo window, with regard to radiation resistance.

IX. APPENDIX

Design Details and Operational Characteristics of the AVCO/Tulsa Space Simulator

A. Ultra-High Vacuum System Description

The vacuum system of the simulator uses a combination of metallic vapor deposition, sputter ion, cryogenic, and physical adsorption processes, thus eliminating the vapor backstreaming and contamination problem of even the most modern of diffusion pump techniques. A schematic of the vacuum enclosure and pumping system is illustrated in Figure 14. A brief description of system components is as follows:

1. Vacuum Enclosure

The main chamber of the system measures approximately 16 inches ID x 18 inches OD x 30 inches high (inside). The chamber walls are constructed with Type 304 stainless steel from a pair of concentric cylinders having a wall thickness of 0.065 inch. The chamber is capped at both ends with metal-to-metal type stainless steel high vacuum seal flanges. The annulus between the chamber walls, except in those regions taken up by feedthroughs and ports into the main chamber, serves as a coolant passage for either water or liquid nitrogen and is also capable of being evacuated to at least 10^{-3} torr with a suitable pump while maintaining a vacuum in the main chamber.

The upper 18 inches of the main chamber contain the working section of the system. Around the mid-periphery of this section, four ports (4 inch nominal on 4-1/2 inch inserts) spaced 90 degrees apart provide a means of introducing samples, radiation and apparatus into the test region and visual check and control of an experiment.

A titanium vapor vacuum pump with an optical baffle to prevent titanium vapor migration into the working section is located in the lower 10 inches of the main chamber. At the base of the working section, in the region just above the optical baffle, ten instrument feedthroughs are introduced into the chamber to provide power, fluids and electrical contact with the test area.

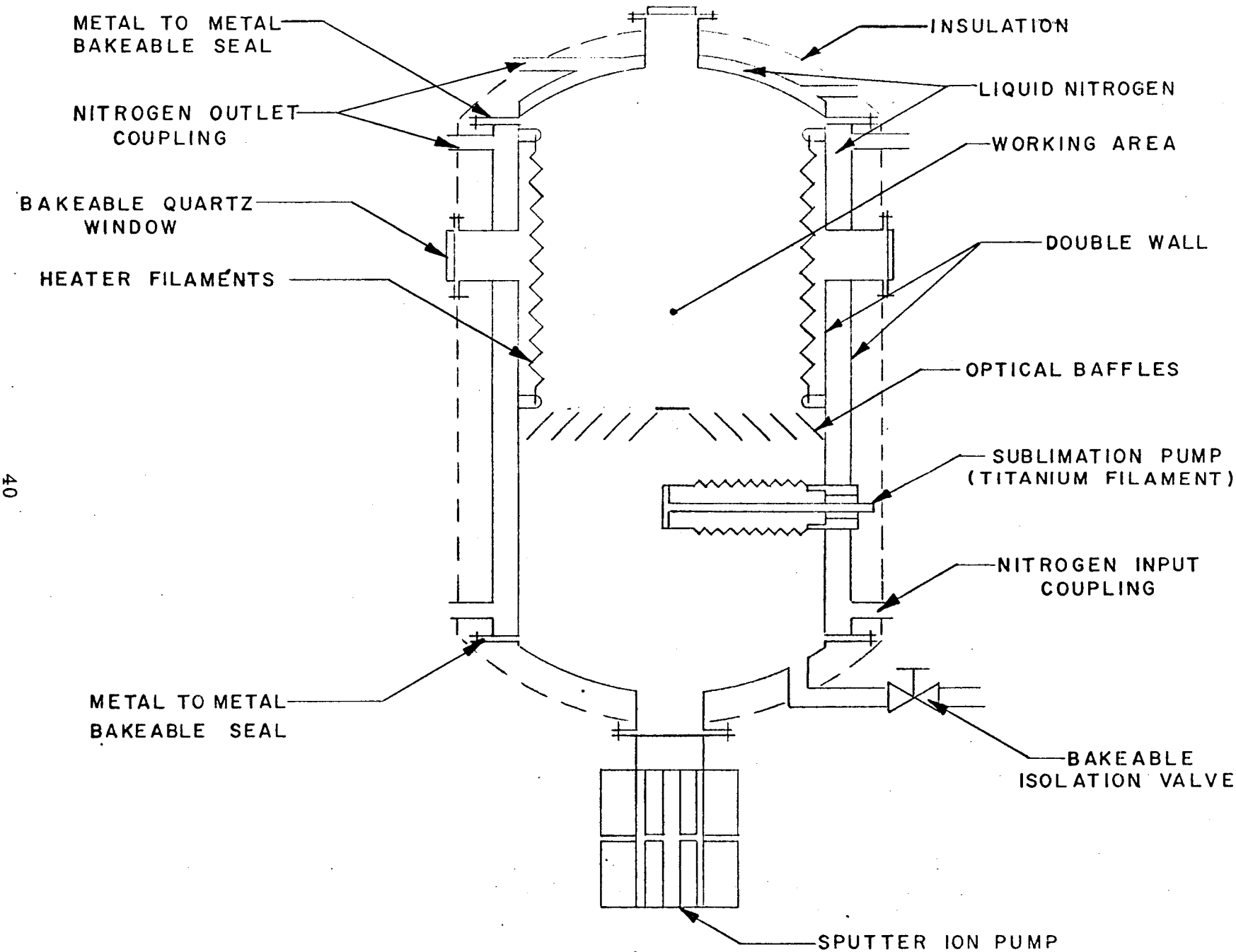

Figure 14 - SCHEMATIC OF ULTRA-HIGH VACUUM SYSTEM

The upper end of the main enclosure is sealed at an all-metal demountable joint with a cover having the same heat transfer and structural requirements as the walls of the system. Another four inch port, identical with those on the walls, is located at the center of the top cover. The construction of the cover allows cooling reservoir characteristics similar to those at the walls of the system. A demountable transition section attached to the all-metal joint at the base of the main enclosure mates with a 400 liter/second sputter-ion pump.

An insulating jacket, which provides easy access to all demountable portions of the main enclosure including ports and feedthroughs and compatible with a maximum temperature of 400° C and a minimum temperature of -200° C, encapsulates the entire chamber, including the chamber-ion pump transition section. The insulation limits the maximum heat flux from room temperature surrounds to 50 Btu/hr-ft^2 with the walls of the system at liquid nitrogen temperature.

Tungsten heater elements are mounted on the inside walls of the working section and have the capability of providing a maximum wall temperature of 400° C in the upper 18 inches of the chamber. A thermocouple to monitor bakeout temperature is mounted in close thermal contact with the inside wall.

2. Pumping System

The primary pump of the system is a titanium sublimation type located in the base of the main chamber. The speed of this pump is approximately 5000 liters/second for nitrogen and approximately 10,000 liters/second for hydrogen. A sufficient number of filament mounts and holders to operate for 340 hours can be inserted through special ports. This pump is complemented by a sputter-ion type of vacuum pump with a pumping speed of 400 liters/second which is attached with a transition section to the bottom of the chamber. The ion pump is bakeable to 400° C with magnets removed. Prior to operating the electronic pumps, the enclosure is roughed to a vacuum of at least 10^{-2} torr by a sorption or a mechanical pump. Hydrocarbons from the mechanical pump are isolated from the high vacuum side of the system by a molecular sieve type of foreline trap. The roughing foreline is introduced into the high vacuum system at the base of the vapor

pump well. An all metal valve capable of being baked at 200° C with the valve closed isolates the high vacuum system from the foreline. There are also two non-bakeable high vacuum valves which are capable of isolating the foreline and sorption pump from the mechanical pump and trap. A thermocouple gauge monitors the foreline pressure of the low vacuum side of the bakeable valve. The mechanical and sorption pumps and trap are mounted on a separate cart and are easily demountable at the bakeable isolation valve.

The main chamber of the simulator is connected to the Van de Graaff vacuum system through a differentially pumped pair of orifices. The differential vacuum system at the orifices is very similar to that used in the main chamber and consists of a 25 liter/second sputter-ion pump in combination with a titanium sublimation pump which has a pumping speed of approximately 300 liters/second on hydrogen.

With the beam on, the Van de Graaff system, which is pumped with oil diffusion pumps, operates with a vacuum of approximately 10^{-5} torr. The differentially pumped orifice section maintains a vacuum of approximately 10^{-7} torr and the main chamber, if the sample is capable of being baked to at least 200° C, will operate in the range from approximately 1×10^{-9} to 3×10^{-10} torr. If the sample is not bakeable, the vacuum in the main chamber at room temperature is limited to approximately 5×10^{-9} torr.

3. Chamber Cart

To allow the precise plumbing of port windows to variable elevations, the design of the cart allows the entire chamber to be rotated plus or minus 90 degrees from the vertical. Mobility and structural integrity of the cart and vacuum chamber are stressed in the design of the system. The rotational motion of the chamber is accomplished in a positive direct fashion with structural rigidity and ease of motion being the most important features of the design. A means of locking the enclosure in a position from vertical to horizontal is provided. The cart is equipped with wheels which have a 360° swivel action and which are also capable of being locked from rolling or swiveling.

4. Target Holder and Apparatus

A number of target holders to maintain thermal control of samples and monitor beam dose have been developed during the past year in support of the programs under way at AVCO/ Tulsa investigating the radiation environment of space. The glass sample holder is illustrated in the inset of Figure 15.

In support of necessary optical measurements, a complete associated spectrophotometer facility is available. Equipment has also been developed to provide in situ measurements of the transmission characteristics of glasses and to provide dynamic, in situ measurements of the thermal characteristics of thermal coatings.

5. Simulator Instrumentation

The rack-mounted controls and instrumentation for the vacuum system, the control console for the Van de Graaff accelerator, control and recording apparatus for the spectrophotometer, and most of the other necessary control and instrumentation equipment are located in a special control room near the simulator facility. This provides for remote control of virtually all phases of operation.

B. Radiation Source Description

1. Xenon-Arc Solar Simulator

The solar simulator covering the wavelength range from 0.2 to 4.0 microns uses a 2 kw. d.c. Ushio High Pressure Xenon Arc Lamp (UXL 2000 DK). Spectral distribution of the radiant emission from this arc is identical to other typical xenon high pressure short arcs. Radiation from the lamp is collected by a 16 inch diameter elliptical mirror coated with a selective front face filter in order to reduce the lamp's excessive emission in the region from 0.8 to 1.1 microns. A fused quartz optical system is provided to transmit the filtered radiation. The output of the optical system is a beam with a maximum average intensity of 1200 w/ft^2 over a four inch working diameter, measured three feet from the exit of the lamp house.

1. Sample Holder
2. Sample
3. Tungsten Screen
4. Metal Sleeve
5. Nickel Photoelectric Probe
6. Glass Sleeve
7. Secondary Electron Collector
8. To Beam Current Readout
9. Liquid Coolant Feedthrough
10. Clamp
11. Monochromator
12. Input Slit
13. Sapphire Window
14. Ultra-High Vacuum Chamber
15. Mirror
16. Deflection Plates
17. Solar Simulator
18. Rotatable Disc
19. Tungsten Source for Transmittance Measurements
20. EUV Source
21. Differential Ion Boostivac Pump
22. Beam Monitor
23. Bellows
24. Differentially Pumped Orifice
25. Valve
26. Analyzer Magnet
27. Diffusion Pump & Baffle
28. Acceleration Tube
29. Gas Source
30. Ion Source
31. Van de Graaff Accelerator
32. UV Port

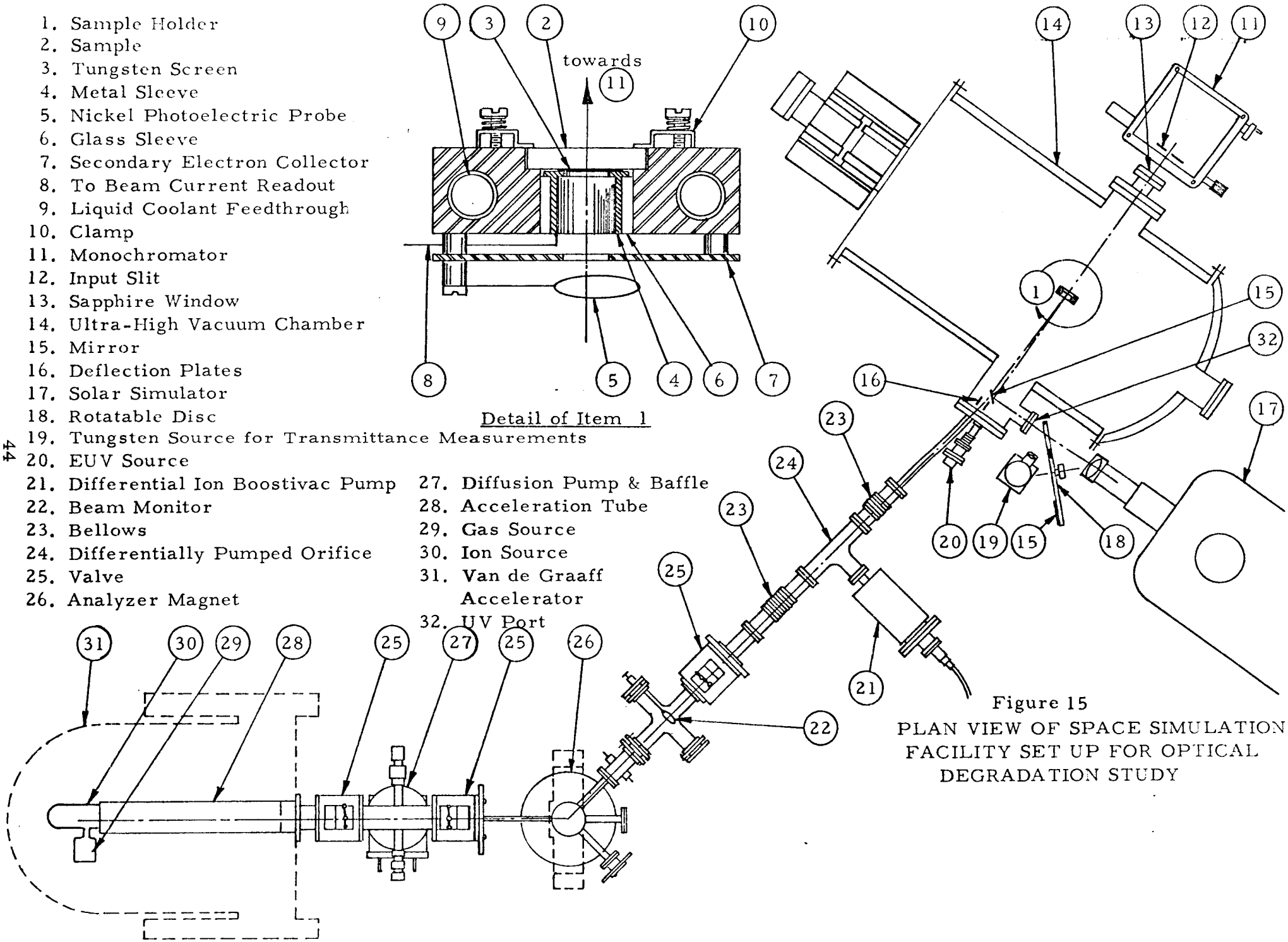

Figure 15
PLAN VIEW OF SPACE SIMULATION FACILITY SET UP FOR OPTICAL DEGRADATION STUDY

The entire lamp house assembly is mounted on a movable tripod pedestal containing adjustable screw jacks. The center line of the exit beam is thus adjustable from 30 inches to 45 inches above floor level. The beam presently enters the chamber through a 2-1/2 inch diameter quartz window.

The lamp is operated from a d. c. power supply. The system includes a control panel with indicators for lamp current, lamp voltage, cumulative lamp running time, number of starts, and radiation intensity. A calibrated monitor to measure the intensity of the output beam is located in an offset position from the optical axis of the beam. Fans for cooling and circulation of air are integrally mounted and are equipped with safety interlocks to assure adequate cooling of the optical system and purging of the ozone created in the lamp house assembly.

2. Vacuum Ultraviolet Solar Simulator

To determine the effects on materials from that part of the solar spectrum between approximately 1000 and 2000 Å, AVCO/Tulsa has developed a vacuum ultraviolet source which has been especially designed to provide collimated, uniform intensities on a sample approximately one inch in diameter. The device utilizes a gas discharge at a pressure of about 10^{-5} torr and is liquid cooled to achieve greater operating power.

At present, the source is being used with hydrogen and a lithium fluoride window which provides an output approximating the solar spectrum from 1050 to 2000 Å. Output of the device is measured with a nitric oxide ionization cell which in turn has been calibrated with a calibrated source at this wavelength.

3. Van de Graaff Generator

The machine can accelerate any positive ion which can be made available to it in the gaseous state. The energy range without an auxiliary power supply extends from a maximum of approximately 0.5 mev to a minimum of 100 kev. By using the accelerating column and ion source of the Van de Graaff with an auxiliary power supply, it is possible to provide an energy range of ions from 3 kev to 100 kev. The

machine is also capable of accelerating electrons over the same range of energies as positive ions. Some modifications are necessary to convert from positive ion to electron acceleration.

The Van de Graaff generator is provided with an analyzing magnet system to provide for mass analysis of the ion beams.

Although the Van de Graaff has been operated primarily in the direct current mode, the machine can be converted to pulsed operation with modifications. Pulse lengths and repetition rates can be varied over a wide range.

REFERENCES

1. Sun, K. H. and Kreidle, N. J., "Coloration of Glass By Radiation," Glass Ind., 33, 511 (1952).

2. Jaffe, L. D. and Rittenhouse, J. B., "Behavior of Materials in Space Environments," JPL TR No. 32-150 (November 1, 1961).

3. "Radiation Effects State of the Art, 1963-1964," Battelle Memorial Institute, Columbus 1, Ohio, REIC Report No. 34 (June 30, 1964).

4. Gigas, G., Ewbank, N. M. and Gruber, D. E., "Interim Report on the Apollo Window Materials Radiation Testing Program," North American Aviation, Atomics International, Canoga Park, California, Al-Memo-9366, Interim Report, 142 pp (February 5, 1964).

5. Kreidl, N. J. and Hensler, J. R., "Formation of Color Centers in Glasses Exposed to Gamma Radiation," J. Am. Cer. Soc., 38, No. 12, (December, 1955).

6. Smith, H. L. and Cohen, A. J., "Color Centers in X-Irradiated Soda-Silica Glasses," J. Am. Cer. Soc., 47, No. 11 (November, 1964).

7. Kats, A. and Stevels, J. M., "Effect of Ultraviolet and X-ray Radiation on Silicate Glasses, Fused Silica, and Quartz Crystals," Phillips Research Reports, 11, 115-156 (1956).

8. Levy, M. and Varley, J. H. O., "Radiation Induced Color Centers in Quartz," Proc. Phys. Soc. B, 68, 223 (1955).

9. Nelson, C. M. and Crawford, J. H., Jr., "Optical Absorption in Irradiated Quartz and Fused Silica," J. Phys. Chem. Solids, 13, 296-305 (1960).

10. Badger, A. E. and Ottoson, A. C., "Effect of Light on Color of Glass," J. Am. Cer. Soc., 25, 104-108 (1942).

11. Hesketh, R. V., "Photo Creation and Destruction of F Centers," Phil. Mag., 4, 8th Ser., 114-125 (1959).

12. Seitz, F., "Color Center in Alkili Halide Crystals, II," Rev. Mod. Phys., 26, 7-94 (1954).

13. Monk, G. S., "Coloration of Optical Glass by High-Energy Radiation," Nucleonics, 10, No. 11, 52-55 (November, 1952).

14. Kreidl, N. J. and Hensler, J. R., "Gamma Radiation Insensitive Optical Glasses," J. Opt. Soc. Am., 47, 73-74 (1957).

15. Hines, R. L., "Radiation Effect of Positive Ion Bombardment on Glass," J. Appl. Phys., 28, 587-591 (1957).

16. Levy, P. W., "Reactor and Gamma-Ray Induced Coloring in Crystalline Quartz and Corning Fused Silica," J. Chem. Phys, 23, 764-765 (1955).

17. Kircher, J. F. and Bowman, R. E., Effects of Radiation on Materials and Components, Reinhold Publishing Corp., New York (1964).

18. Rindone, G. E., "The Formation of Color Centers in Glass by Solar Radiation."

19. Cooley, W. C. and Janda, R. J., "Handbook of Space-Radiation Effects on Solar Cell Power Systems," NASA SP-3003 (1963).

20. Hess, R. E., "Space Radiation as an Environmental Constituent," REIC Memo No. 19, Battelle Memorial Institute, Columbus, Ohio, (January, 1960).

21. Redmond, R. F., "Space Radiation and Its Effect on Materials," REIC Memo No. 21, Contract AF33(616)-7375 (June 30, 1961).

22. Hess, W. N., "Earth's Radiation Environment," Space/Aeronautics, 68-76 (November, 1964).

23. Burrill, E. A., "Simulating Space Radiation," Space/Aeronautics, 78-87 (May, 1964).

24. Roberts, W. T., "Space Radiations: A Compilation and Discussion," NASA TM X-53018 (March 5, 1964).

25. McIlwain, C. E., "The Radiation Belts, Natural and Artificial," Science, 142 (October 18, 1963).

26. Electro-Optical Systems Report, "Study of a Flight Experiment of Solar-Concentrator Reflective Surfaces,"a report to NASA, NASA CR-55893, Contract NAS1-2880, 2-2 thru 2-34 (November 1, 1963).

27. STL Report TR 9990-6032-RU000, "Equipment Design Considerations for Space Environment" (June 6, 1962).

28. McIlwain, C. E., "Coordinates for Mapping the Distribution of Magnetically Trapped Particles," J. Geophysical Res., 66, No. 11 (November, 1961).

29. McDonald, F. B., "Solar Proton Manual," NASA TR R-169, Washington, D. C. (September, 1963).

30. Madey, R., "A Useful Formula for Calculating Space Proton Dose Rates," Trans. Am. Nuclear Soc., 6, 2 (1963).

31. Madey, R., et. al., "Proton Dose Rates in Manned Space Vehicles," Am. Astronautical Soc., preprint, 62-22 (1962).

32. Madey, R., "Shielding Against Space Radiation," Nucleonics (May, 1963).

33. Arnoldy, R. L., Hoffman, R. A. and Winckler, J. R., "Solar Cosmic Rays and Soft Radiation Observed at 5,000,000 Kilometers from Earth," J. Geophys. Res., 65, 3004-3007 (1960).

34. Van Allen, J. A., "Analysis of Space Radiation Phenomena," paper presented to IAS Symposium on Manned Space Vehicles.

35. Winckler, J. R. Bhavasar, P. D. and Peterson, L., "Time Variation of Solar Cosmic Rays During July, 1959 at Minneapolis," J. Geophys. Res., 66, 995-1022 (1961).

36. Dorman, L. I., Cosmic Ray Variations, State Publishing House for Technical and Theoretical Literature, Moscow (1957).

37. Parker, E. N., "Hydrodynamic Theory of Solar Corpuscular Radiation and Stellar Winds," Astrophys. J., 132, 821-861 (1960).

38. Dessler, A. J., Penetrating Radiation, edited by F. S. Johnson, Stanford University Press, Stanford, California.

39. Van Allen, J. A., "Brief Note on the Radiation Belts of the Earth," T.I.D. 7652, Book 1 (November, 1962).

40. Whipple, F. L., J. Geophys. Res., 68, No. 17, 4929-4939 (September, 1963).

41. Johnson, F. S., "The Solar Constant," J. of Meteorology, 11, 431-439 (1954).

42. Friedman, H., "Rocket Spectroscopy," Space Science, John Wiley, 549-627 (1963).

43. Hess, W. N., "The Artificial Radiation Belt Made on July 9, 1962," J. Geophys. Res., 68, 619 (1963).